Flow dynamics and tributary mouth bar formation at river confluences with high rates of tributary sediment supply

G. Moradi[1], C.D. Rennie[2] and S.N. Lane[1]

[1]Institute of Earth Surface Dynamics, Université de Lausanne, CH1015 LAUSANNE, Switzerland
[2]Civil Engineering Department, University of Ottawa, OTTAWA, Canada
Corresponding author: Gelare Moradi (gelare.moradi@unil.ch)

Key Points:

- Angular momentum ratio rather than momentum ration may be a better means of classifying river junctions.
- Tributary-attached bars can lead to secondary circulation even at low angular momentum ratios.
- Coarse-grained tributary-attached bars may from main channel rather than tributary sediment.

Abstract

River confluences influence the formation of secondary circulation, bed morphology, and associated feedbacks. With distance downstream through a drainage network, it becomes likely that the flow momentum of tributaries is lower than that of the main river, creating confluences with very low momentum ratio. However, the tributary may be able to supply significant quantities of sediment, especially in watersheds with high relief. High flow and sediment supply events in the tributary may decouple in time from those in the main river. The capacity of the main river to evacuate tributary-delivered sediment may occasionally be lower than the sediment delivery rate. The result is the formation of confluences with large tributary mouth bars that may influence confluence flow structures even when the tributary discharge has declined. There are no field examples measured to date for such confluences. Here, we report the first field data for three such river confluences, along the upper Rhône River, Switzerland. We combine aDcp measurements with the analysis of the provenance of sediments in the tributaries and main stem. We introduce the angular momentum ratio for confluence classification. The formation of tributary mouth bars and a scour hole was identified for the two junctions with significant tributary sediment supply. These bars were sufficient to introduce secondary circulation even at very low flow momentum ratios. The analysis of sediment provenance suggested that the origin of the bars was not necessarily the tributary but could be a consequence of the effects of the tributary upon main channel sediment routing.

1 Introduction

Flow dynamics at the junction or confluence of two river channels is characterized by the formation of secondary flow. Extensive research has quantified this formation (e.g. Mosley, 1976; Best, 1987,1988; Rhoads and Kenworthy, 1995,1998; Biron, 1996; Biron et al., 1996a,1996b; Rhoads and Sukhodolov, 2001,2008; Rhoads et al., 2009; Constantinescu et al., 2011,2012; Leite Ribeiro, 2011; Konsoer and Rhoads, 2014; Lewis and Rhoads, 2015; Riley et al., 2015; Rhoads and Johnson, 2018; Yuan et al., 2021; Li et al., 2022) and attempted to establish what controls it. The momentum ratio (M_r):

$$M_r = \frac{Q_t U_t \rho_t}{Q_m U_m \rho_m} \quad (1)$$

where Q, U and ρ are discharge (m^3s^{-1}), mean flow velocity (ms^{-1}), flow density (kgm^{-3}), t and m refer to the tributary and main channel, respectively; has been identified as a critical control on the secondary circulation that forms. Its implications for the rate of mixing of the two confluent channels and for stream bed erosion have been demonstrated (e.g. Kenworthy and Rhoads, 1995; De Serres et al., 1999; Bradbrook et al., 2001; Lane et al., 2008; Rhoads et al., 2009; Constantinescu et al., 2012; Riley and Rhoads, 2012; Riley et al., 2015; Lewis and Rhoads, 2015; Rhoads and Johnson, 2018; Tang et al., 2018). There remain fewer studies of how junction morphology evolves as M_r changes (but see Mosley, 1976; Ashmore and Parker, 1983; Best, 1988; Ashmore et al., 1992; Boyer et al. 2006; Rhoads et al., 2009). A dominant but not exclusive focus on self-formed confluences in laboratory settings has described the mutual adjustment between confluence morphology, flow processes and sediment transport. However, and notably in large river basins, the timing of tributary sediment supply may not be the same as in the main channel, leading to a disequilibrium between the tributary flow, the main channel flow and the confluence morphology. High flow and sediment transport events in the tributary may mean that for short time periods the tributary can deliver significant amounts of coarse sediment to the main channel and/or influence the routing of main channel sediment through the junction. Both can have geomorphological consequences, notably the formation of a tributary mouth bar (e.g. Biron et al., 1993; De Serres et al., 1999) which may extend into the main stem to form a bar attached to the downstream junction corner (Best, 1988; Guillén-Ludeña et al., 2015, 2016, 2017; Leite Ribeiro et al., 2012). Although these are likely to be formed during high flow events in the tributary, the bars themselves may remain in the main stem for some time, leading to a confluence morphology that is not completely adjusted to M_r values at low flows. This is particularly the case where steep tributaries enter main rivers, such as in watersheds with a high relief, and the material can be very coarse. The associated deposits may require shear stresses for entrainment substantially greater than those typical of the main stem.

Figure 1 shows three examples of such confluences in the Swiss River Rhône. These tributary mouth bars constrict the post confluence channel (Figure 1), causing the main stem to curve in the same sense as the tributary. Thus, it is possible that even if the M_r between the tributary and main stem is very low indeed, where there are “legacy” tributary mouth bars, secondary circulation could form, and this could influence mixing and bed sediment transport through the confluence, as well as the long-term stability of the tributary mouth bar itself.

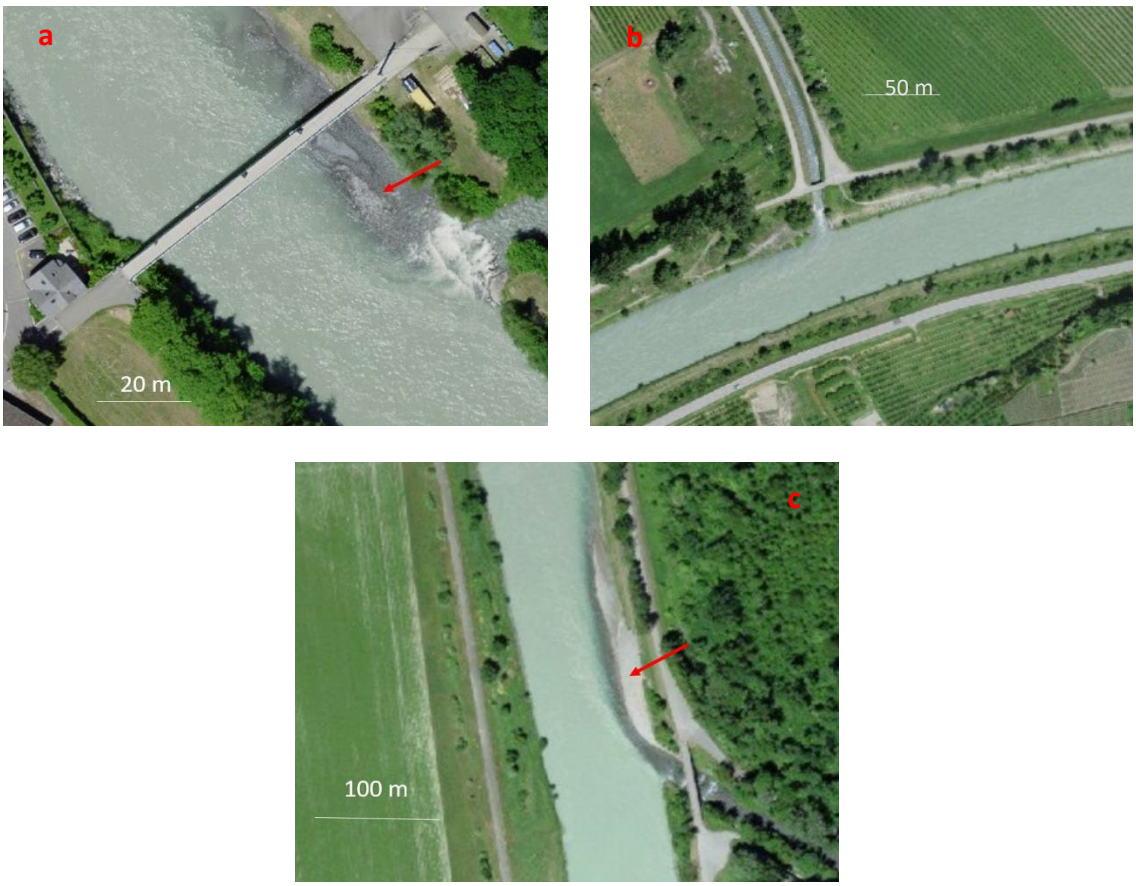

Figure 1. Three examples of confluences in the Swiss River Rhône a. the Avançon; b. the Lizerne and c. the Grande Eau. The Avançon and the Grande Eau have tributary mouth bars attached to the downstream corner junction (annotated with red arrows) with sediment transport in the tributary. Sediment delivery in the Lizerne is limited due to upstream hydropower exploitation.

It is not clear whether these mouth bars form due to high sediment loading from the tributary (Guillen Ludena et al., 2017); or from a high flow in the tributary that influences sediment routing in the main stem, causing mouth bar formation from main stem sediment. The latter may be encouraged due to discordance between the tributary and the main stem, such that the tributary flow enters as a jet (Sukhodolov et al., 2017), with deceleration (Riley et al., 2015) and upwelling of main stem flow downstream of the junction corner (Guillén-Ludeña et al., 2016a).

Significant progress has been made in studying the hydraulics and morphodynamics of tributary junctions with low momentum ratios but where there is a relatively high rate of sediment delivery from the tributary (Leite Ribeiro et al., 2012; Guillén Ludena, et al., 2015; 2016; 2017). These have predominantly focused on laboratory studies. There have been very few studies of such junctions in field environments, notably where there is a low flow in the tributary, and no sediment supply, leading to extremely low M_r (< 0.05). Leite Ribeiro et al. (2012) undertook an experiment with M_r = 0.02 but a high rate of tributary-delivered, poorly-sorted sediment. They showed that these conditions led to hydrodynamics that were different to existing conceptual models. They concluded that the most unusual characteristic of confluences with low momentum ratios and high rates of sediment supply is the formation of a pronounced bed discordance in the confluence zone associated with the formation of a tributary mouth bar. The discordance leads to a two layer-flow structure downstream of the junction. The flow from the

tributary mainly penetrates as a jet in the upper part of the water column. A horizontal recirculation zone does not necessarily form downstream of the junction corner. Rather, the main stem flow is accelerated under the tributary jet and then decelerates and upwells downstream of the junction downstream corner (Guillén Ludena, et al., 2015). If the tributary momentum decreases, the tributary mouth bar progrades into the main stem (Guillén Ludena, et al., 2016) although this is in contrast to what others have observed (Best, 1998; Biron et al., 1993; Riley et al., 2015). The height of the bank attached tributary mouth bar appeared to be lower for higher momentum ratios (Guillén Ludena, et al., 2016).

Flow curvature from the tributary into the main channel will lead to a centrifugal force that is not taken into account by consideration of momentum alone. For this reason, the centrifugal force across the stream width should be integrated meaning the calculation of an angular correction factor A. Herein, we introduce this factor to modify the momentum ratio to what is effectively an angular momentum ratio (M_{ar}).The laboratory observations of Leite Ribeiro and Guillén Ludena and their colleagues imply that the tributary mouth bars that form at confluences with very low momentum ratios are going to relate to interactions between main stem and tributary flow and sediment transport, which vary with flow stage. However, these processes remain unclear and have yet to be observed in the field. Also, they did not consider the effect of the angular momentum in correcting the momentum ratio. Accordingly, this paper tests three hypotheses: (1) that due to the legacy of high tributary sediment delivery, tributary mouth bar formation can lead to significant secondary circulation even at very low M_r conditions; (2) that these tributary mouth bars form from both main flow and tributary supplied sediment; and (3) the junction angle can lead to a centrifugal force that should be taken into account through a corrected M_r

1 Methodology

The focus of the data collection is three junctions of the Swiss River Rhône. In this section, we describe and justify the choice of these junctions and explain the measurements and processing steps adopted.

2.1 Study Site

The tributaries are all in a sector of the river that has been extensively straightened for flood control and each tributary is engineered to enter the main stem at a high angle (between 70^o and 90^o). Thus, they are not dissimilar to the design of laboratory experiments used to inform some of our understanding of river confluence hydrodynamics (e.g. Best, 1987, 1988; Biron et al., 1993; Leite Ribeiro et al., 2012; Guillén Ludena, et al. 2015, 2016). The three tributaries were chosen on the basis of: (1) having low flow momentum ratios for most of the time (< 0.05); (2) having high sediment supply rates in two cases, the third having a gravel trap and sediment extraction upstream, negligible sediment supply and thereby providing a controlled comparison; (3) high junction angles; and (4) suitability for sediment provenance analyses so the origins of the sediment that comprised the tributary mouth bars could be determined. The three junctions studied were: (1) the Avançon-Rhône confluence, (2) the Lizerne-Rhône confluence and (3) the Grande Eau-Rhône confluence (Figure 2). The basic characteristics of these three confluences are given in Table 1 and Figure 3.

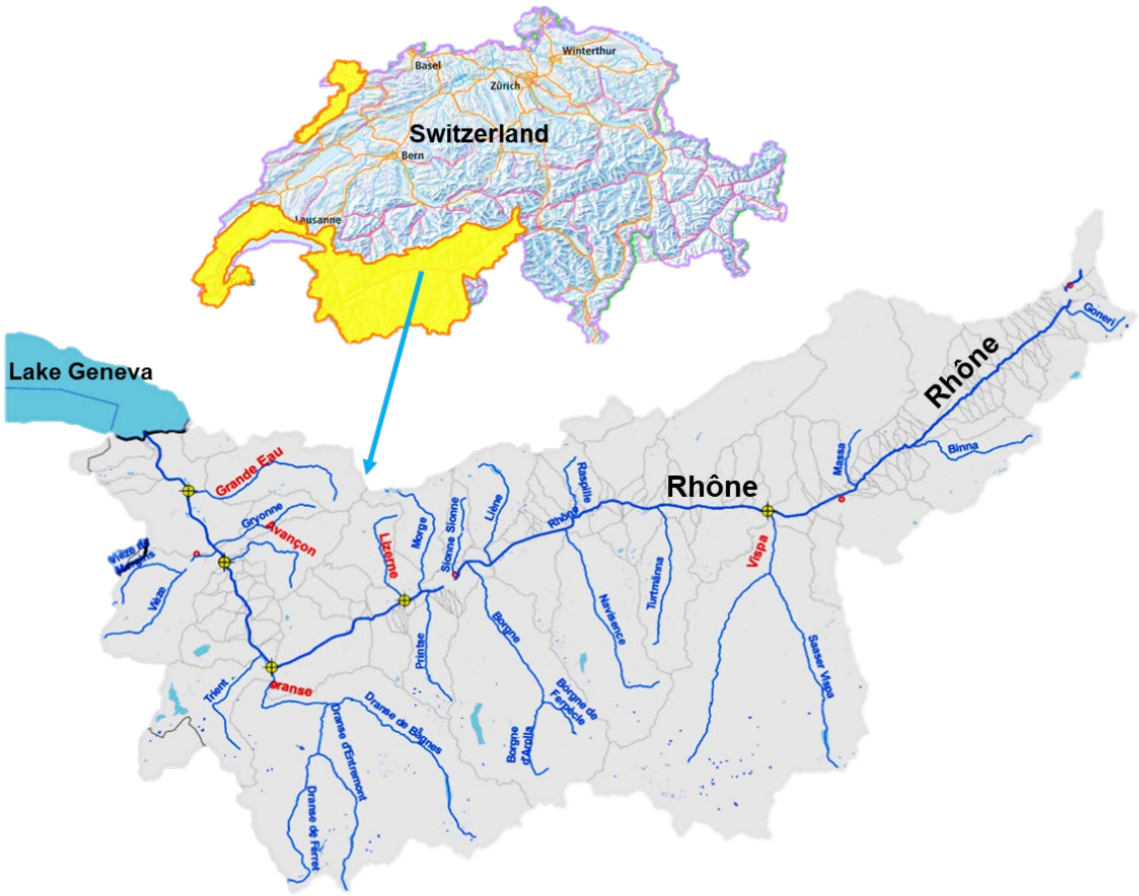

Figure 2. Location of the three studied river confluences

Sites	Avançon	Lizerne	Grande Eau
Measurement date	16.10.2017	07.08.2017	23.05.2018
Tributary upslope contributing area (km^2)	87.5	64.8	132
Main stem upslope contributing area (km^2)	4402	3401	5088
Basin area ratio	1.99%	1.89%	2.59%
Tributary width (m)	8.5	6.5	16.5
Main stem width upstream of junction (m)	54	40	58
Main stem width downstream of junction (m)	56	52	60
Width ratio	0.18	0.15	0.28
Tributary mean depth at the junction (m)	0.2	1.4	0.8
Main stem mean depth upstream of junction (m)	1.5	1.9	2.4
Main stem mean depth downstream of junction (m)	3.1	2.5	3.5
Junction angle (º)	90	80	70
Tributary Froude number (Leite Ribeiro, 2011)	0.56	0.32	0.15
Bed slope of the tributaries upstream of the confluence (%) (Leite Ribeiro, 2011)	<1.5	~0.5	0.5-1
Main stem slope upstream of the confluence (%)	0.9	2	2.2
Tributary slope at discordant bed into main stem (°)	29.8	33.1	26.6
Discharge ratio during measurement	0.018	0.012	0.027
Momentum ratio during measurement	0.021	0.018	0.022
Radius of main channel curvature (°) (see section 2.4)	60.3	46.5	76.5
Angular momentum ratio during measurement (see section 2.4)	0.019	0.015	0.017

Table 1. Selected upper Rhône tributaries with their typical characteristics on the day of measurements.

Figure 3 shows the historical daily mean discharge values for a period of 3 years for the Avançon (Figure 3a) and the Grande Eau (Figure 3b). The values of daily mean discharges for the measurement dates for both confluences are indicated on the graphs. As compared with the measurement dates (Table 1) the last likely tributary-dominant event for the Avançon (Figure 3a) was on June 4th, 2017, with a discharge of 11.1 m^3s^{-1}. The measurement duration of the Avançon is too short to estimate a return period for the June 2017 event, but the closest rain gauge suggests that the daily rainfall on the 4th of June was higher than 95.8% of daily rainfalls in the period 1998-2018. This confluence was measured on the 16th August 2017 (Figure 4a) when the momentum ratio according to (1) was 0.021.

The Lizerne (Figure 4b) is heavily regulated for hydropower with sediment extracted upstream of the junction (~3 km upstream of the junction). As a result, there is negligible sediment supply and no evidence of tributary mouth bar formation. Field data were collected on August 7th, 2017 with an M_r of 0.018. There are no historical hydrological data for the tributary.

For the Grande Eau the last likely event before the date of measurement was January 5th, 2018 (Figure 3b), with a discharge value of 24.9 m^3s^{-1} and a return period of around 2 years (Source OFEV). The confluence was measured on the 23rd May 2018 when *Mr* was 0.022 (Figure 4c).

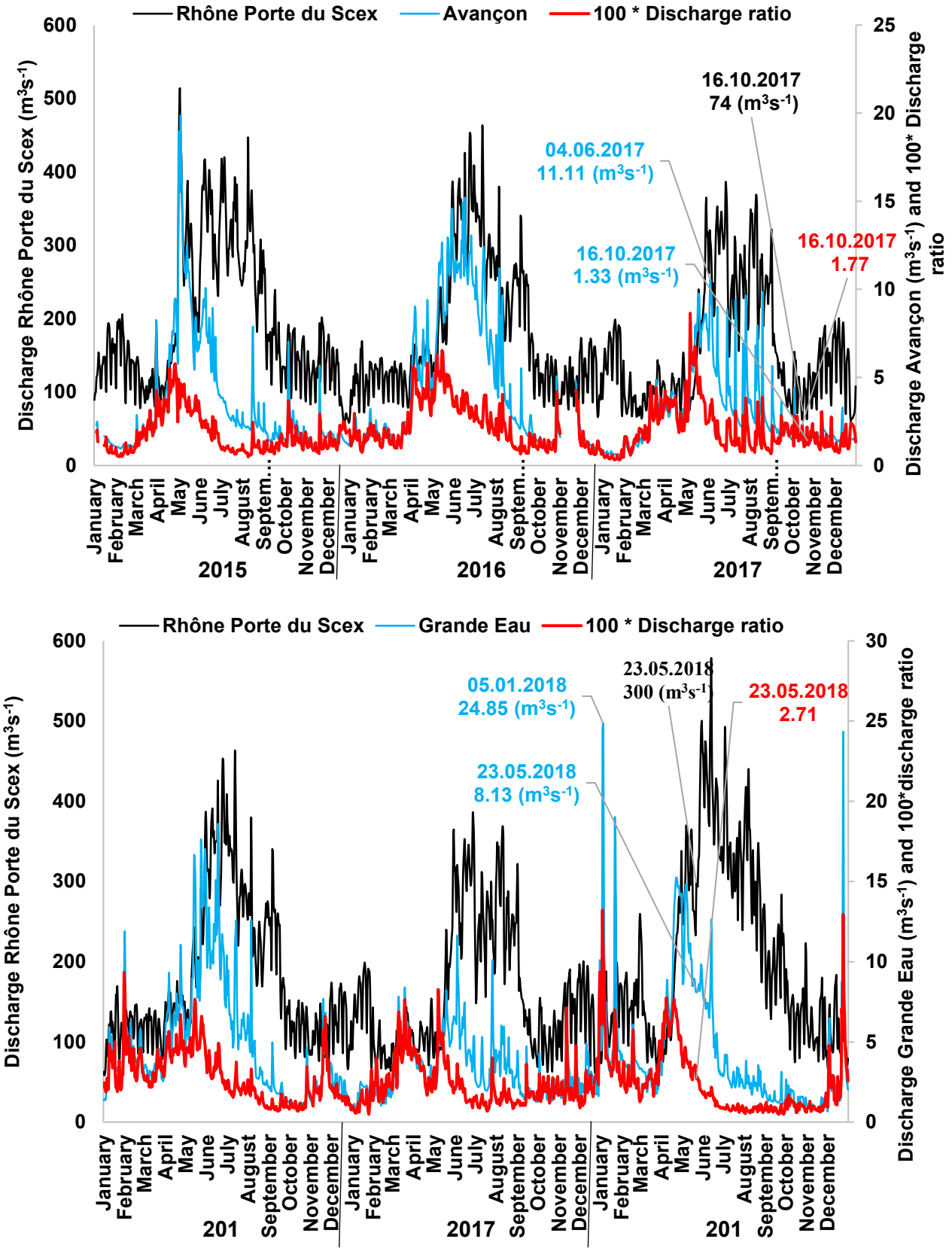

Figure 3. Daily mean discharge values for the Avançon (3a) in 2017 and the Grande Eau (3b) in 2018 (Source OFEV) with their discharge ratios. The Lizerne discharge is not measured.

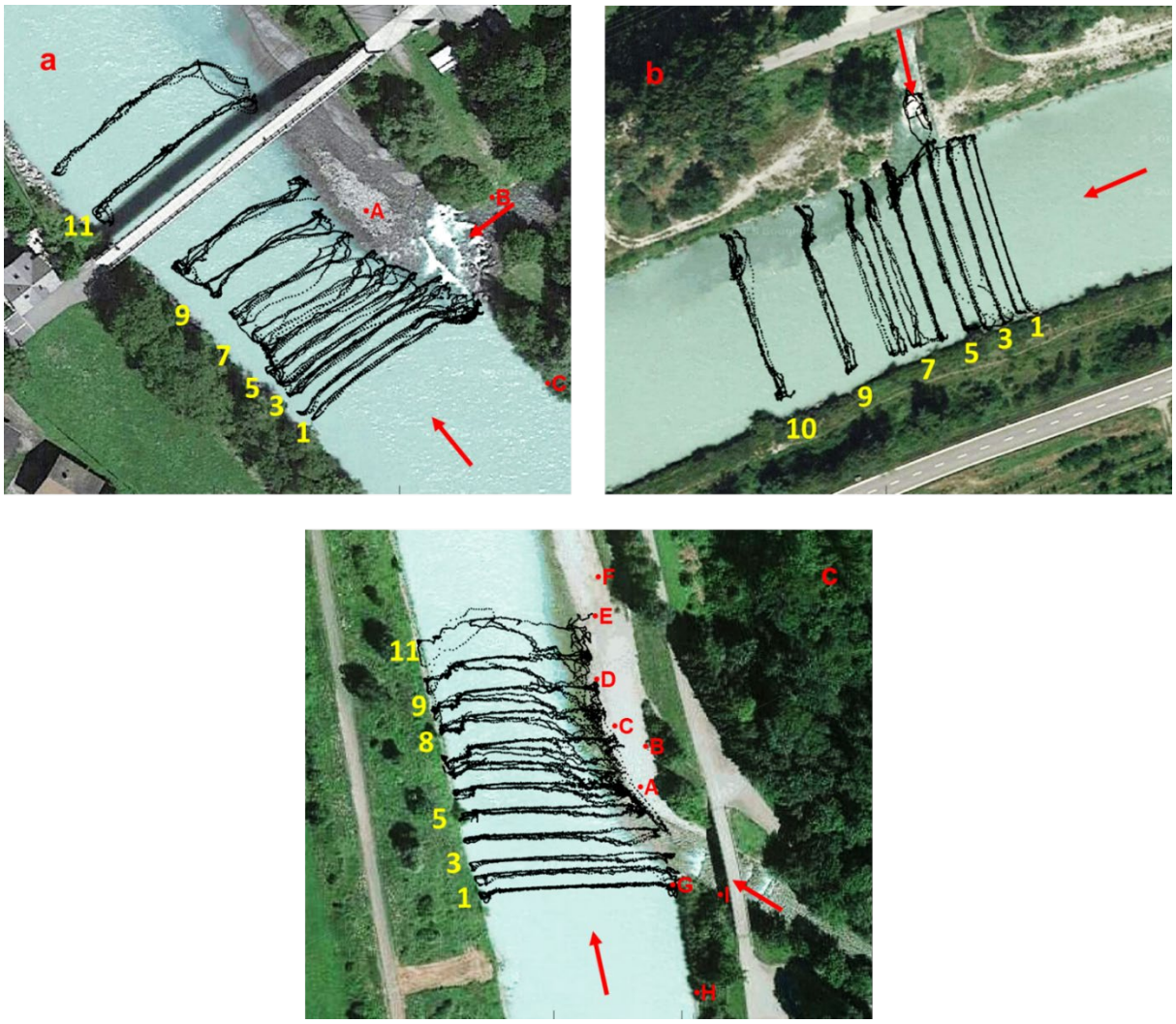

Figure 4. Location and surveyed cross sections at a) Avançon-Rhône confluence (October 2017), b) Lizerne-Rhône confluence (August 2017) and c) Grande Eau- Rhône confluence (May 2018) and selected cross sections for primary and secondary flows representation. Red points are the sediment samples

2.2 Angular momentum ratio calculation

The calculations for momentum ratio presented in Section 2.1 were based upon (1). However, they have different junction angles (Figure 4). Theoretical analyses show that the intensity of secondary circulation in a river is influenced by curvature (Dietrich and Smith, 1983) and hence as junction angle changes, so the degree of curvature changes. To allow better conference comparison we here introduce the angular momentum ratio. The angular momentum ratio is based upon taking into account the centrifugal force which is produced by the curvature of the flow from the tributary into the main channel. For this reason, the angular correction factor (A) is calculated for all three tributaries by integrating the centrifugal force across the stream width (W) using:

$$A = \frac{r_1}{r_2} \tag{2}$$

where r_1 and r_2 are the radii of the main channel curvature (m) and tributary curvature respectively. If each channel has curvature at the confluence mixing zone, then r_1 and r_2 in

equation 2 should be perpendicular to the flow path of the respective channel. As the main channel is straight at all three junctions, r_1 tends to infinity. To be able to compare these three confluences, it is assumed that r_1 is equal to the width of the main channel upstream of the junction (w) and the correction is only applied to the tributaries. Applying (2) needs determination of r_2 on the basis of the junction angle (θ). Whilst the junction angle is readily measurable, the radius of curvature can only be determined from the junction angle if there is some length scale specified over which the tributary must turn. It is argued here that this length scale should be based upon the width of the main channel downstream of the junction (W_1) and the width of the tributary (W_2) (see Figure 5).

$$r_2 = \sqrt{W_1^2 \times W_2^2 - 2 \times W_1 \times W_2 \times cos(180 - \theta)} \quad (3)$$

This ratio then is used to obtain the angular momentum ratio (M_{ar}):

$$M_{ar} = A \times M_r \quad (4)$$

Table 1 gives the angular momentum ratio, showing how this correction increases the momentum ratio in the Avançon and the Lizerne as compared with the Grande Eau. This is due to the smaller junction angle at the Grande Eau which leads to a smaller penetration of the tributary into the main channel.

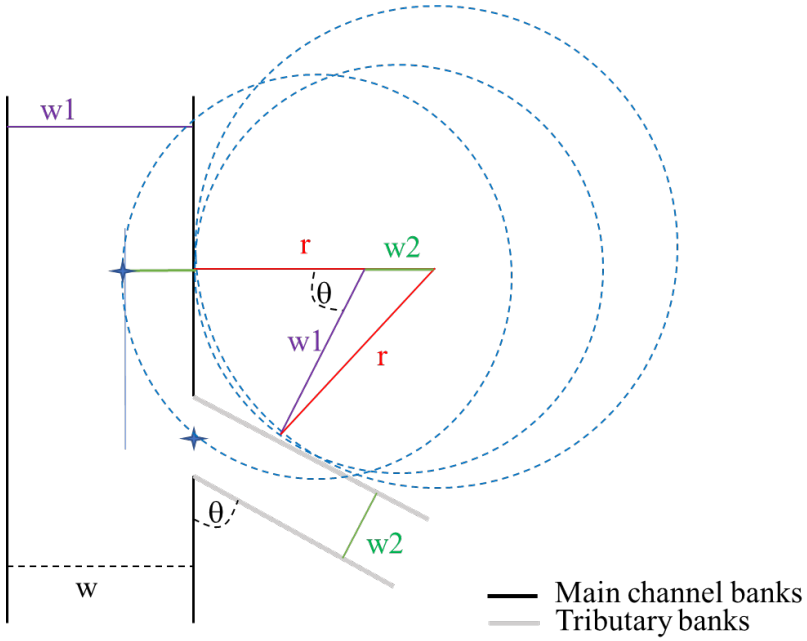

Figure 5. Schematic of angular momentum calculation

Angular momentum ratios for the Grande Eau from 2016 to 2018 can be calculated by applying the angular factor to correct the momentum ratios determined using historical water level data, assuming that the section is rectangular, so the width is constant. Figure 6 shows the frequency plot of the calculated angular momentum ratio. A similar analysis was not possible for the Avançon junction due to only discharge data being available.

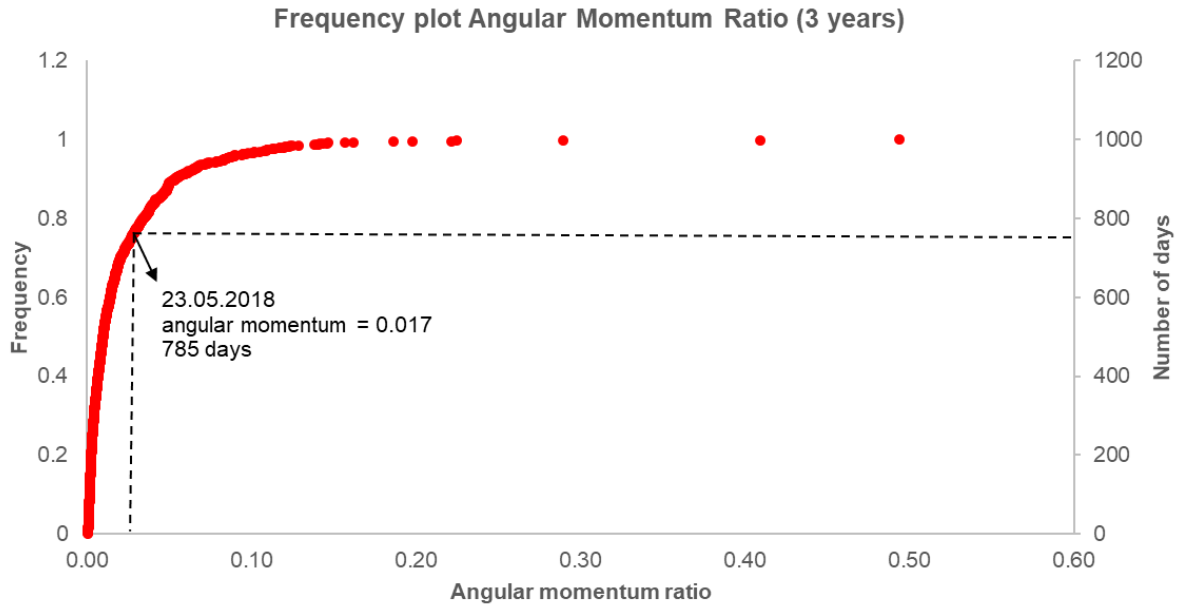

Figure 6. Frequency plot for angular momentum ratio for the Grande Eau from 2016 to 2018

2.3 Velocity and bathymetric data collection

At each confluence, the measurement of the bathymetry and the time-averaged flow velocities and flow discharge at several cross sections through the confluence was performed using a moving boat acoustic Doppler current profiler (aDcp) system. This system has proven to be a reliable means of estimating the mean discharge and velocity in rivers. This method can be used not only to estimate the discharge (e.g., Parsons et al., 2005; Kostaschuk et al., 2009; Gunawan et al., 2010; Shugar et al., 2010; Sassi et al., 2011) but also local bed shear stress (τ) (e.g., Sime et al., 2007; Petrie et al., 2010; Rennie and Church 2010), sediment transport (e.g., Gartner, 2004; Rennie and Villard, 2004; Rennie and Millar, 2004; Kostaschuk et al., 2005; Parsons et al., 2005) and secondary circulation (Dinehart and Burau, 2005; Szupiany et al. 2007; Venditti et al. 2014). The aDcp was a Sontek RiverSurveyor M9, which sets beams at 25° angle from vertical. It was trimaran mounted and synchronized with a differential Global Positioning System (dGPS). This system has a profiling range of 0.06 to 40m and can measure a velocity range of ± 20 ms^{-1} in vertical bin cell sizes ranging from 0.02 to 4 m. The aDcp measurements of depth and velocity were made in single ping ensembles using 10 cm long bins.

A specially-designed rope pulley system (Figure 7) was set up for cross-sections, each perpendicular to the main Rhône with a 0.1w spacing (w is the post confluence river channel width) to a distance 2w downstream of the downstream junction corner. It is impossible to maintain even partly straight lines with a motorized boat in this kind of stream. Figure 4 shows that certainly for the Avançon (Figure 4a) and the Lizerne (Figure 4b) it was possible to use the pulley to reproduce the same traverse of each section. For the Grande Eau (Figure 4c), due to the distances involved, coupled to the increased width of the main stem, this was less the case, and this may introduce some error into the Grande Eau results. Following the recommendations of Szupiany et al. (2007), the cross-sectional measurements were made by conducting six traverses along each cross section.

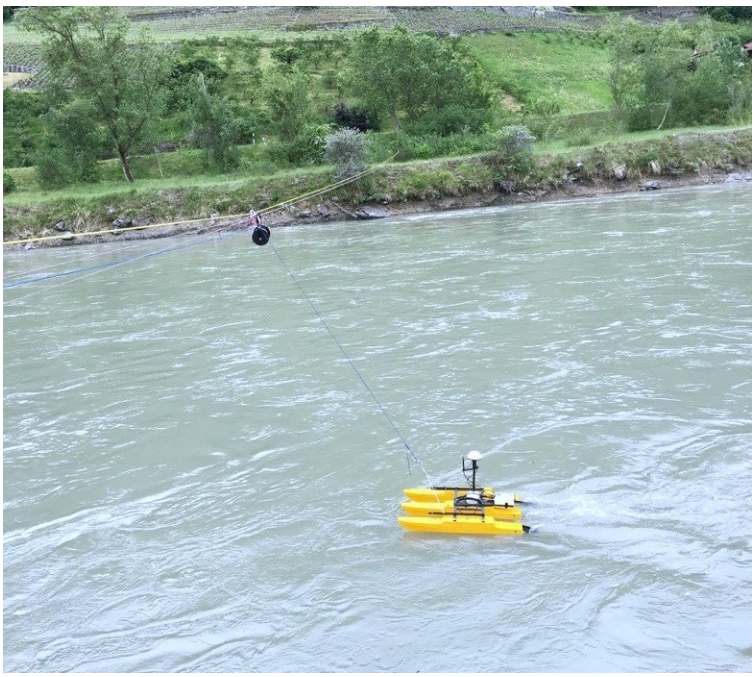

Figure 7. Rope-pulley system, illustrated for the Lizerne

2.4 Velocity and bathymetric data processing

The aDcp data collected at each confluence were first processed to yield spatially-distributed maps of bathymetry, near-surface velocity, and near-bed velocity. The water depth and profile of three dimensional (3D) Cartesian velocities (east, north, and up components) collected at all aDcp measurement points were extracted and processed in Matlab. Along with the water depths, the east and north velocity vector components and the 3D velocity magnitude in the bins nearest the water surface and nearest the bed were then interpolated using Kriging in Surfer software to generate spatial maps of these quantities.

Secondary flow circulation at individual transects was identified using the beam velocity method (Vermeulen et al. 2014b) aided by the repeat surveys of each transect (Figure 4). A full description and evaluation of this method is given in Moradi et al. (2019) and only a brief explanation is provided here. An aDcp measures the radial beam velocities (**b**), i.e., the projections of the local velocity vectors in the direction of each acoustic beam (**q**). To determine Cartesian velocity components (v_x, v_y and v_z), these radial velocities have to be resolved into three orthogonal velocity vectors. These velocities should then be corrected for pitch and roll angles, obtained from the aDcp's internal inclinometer and heading angle from the aDcp's internal compass. The method introduced by Vermeulen et al. (2014b) was used to transform radial beam velocities measured within a velocity bin to Cartesian velocity components, using the following equation:

$$\begin{pmatrix} b_1 \\ \vdots \\ b_N \end{pmatrix} = \begin{pmatrix} q_1 \\ \vdots \\ q_N \end{pmatrix} . \begin{pmatrix} v_x \\ v_y \\ v_z \end{pmatrix} \leftrightarrow \boldsymbol{b} = Q . \boldsymbol{u} \tag{5}$$

Since there is always some measurement error due to instrument noise, the above equation can be rewritten as:

$$\boldsymbol{b} = Q\boldsymbol{u} + \varepsilon \tag{6}$$

where ε is the error term. A least squares solution can be then fitted to (6) that minimizes the sum of the square of the errors. The optimal velocity estimation ($\hat{u}$) for ($\vec{u}$) is then given by the normal equation:

$$\hat{u} = Q^{+}\boldsymbol{b} + \varepsilon \tag{7}$$

The error term also includes information about the turbulence and accuracy of the measurements. The covariance matrix of the velocity components can be obtained using the following equations:

$$\hat{\varepsilon} = \boldsymbol{b} - Q\hat{u} \tag{8}$$

$$var(\hat{u}) = \frac{\hat{\varepsilon}^T \hat{\varepsilon} (Q^T Q)^{-1}}{N - 3} \tag{9}$$

and the variance of the velocity across the section can then be estimated as:

$$var(u) = \frac{var(\hat{u})}{N} \tag{10}$$

As the instrument is mounted on a moving boat, corrections should be made for boat velocity in order to obtain absolute water velocities. The boat velocity is determined either by bottom tracking (BT) or by use of differential Global Positioning System (dGPS) data. Boat velocity measurement by bottom tracking is typically more accurate than by dGPS, but bottom tracking for water velocity measurement is limited to immobile bed conditions. Bottom tracking involves measurement of the Doppler shift in the frequency of an independent echo sounding off the bed. If the bed is stationary, the shift in frequency is proportional to the boat velocity. However, if the bed is mobile then bottom tracking is biased by the sediment motion and the frequency shift is due to both the boat velocity and the sediment motion. In this study, the boat velocity measured by dGPS is used because of the possibility of the bed being mobile.

The basic bathymetric model is estimated using the UTM positioning of the bed elevation data collected with the aDcp and a LOWESS interpolation model (Moradi et al. 2019), which has the effect of defining a bathymetric model that gives most weight to points that appear to be closer to the measured points. For each cross section, a best-fit section line is also defined using the UTM positions of the bed elevation of all six repeat transects, estimated using the bathymetric model. Using this best fit cross-section, a cross-section mesh is then generated and measured beam velocities are projected onto this mesh. Cartesian velocity components are then calculated for each mesh cell using the procedure defined above. The beam velocity processing method yielded calculated Cartesian velocities at each point in the cross-section mesh. Moradi et al. (2019) has used the same approach for the Avançon and the Lizerne and has reported that using this new method improves significantly the results obtained for secondary circulations. Primary and secondary velocity vectors were then estimated, based on the assumption that the secondary currents in one direction are balanced by those in opposite direction, to produce zero secondary discharge for a given profile. Finally, the secondary velocities were evaluated for the presence of helical cells. At the confluence of two rivers, the large-scale helical cells can interact and form the smaller scale secondary circulation cells within their mixing interface. These small-scale helixes are known as streamwise oriented vertical (SOV) cells (Sukhodolov and Sukhodolova, 2019)

2.5 Analysis of sediment provenance

The study was interested not only in the flow structures that formed in the presence of tributary mouth bars at very low flows, but also the origin of the tributary mouth bars themselves. Reflecting the severe difficulty of measuring coarse sediment transport in the junction during extreme tributary flows, the study sought to attribute tributary mouth bar formation to sediment sourced from the tributary versus sediment sourced from the main stem, as this would allow inference of possible sediment transport paths during tributary mouth bar formation.

The upper Rhône River basin comprises three litho-tectonic units with different geological histories (Stutenbacker et al., 2018). The External Massifs include autochthonous slices of crystalline basement (Herwegh et al., 2017) as well as some "sub-penninic" (i.e. allochthonous) basement nappes containing mostly metagranites and gneisses (Stutenbacker et al., 2018). The Penninic nappes include: (1) ophiolites of the Valais and Piedmont-Liguria oceans (metabasalts, metagabbros, serpentinites, calcschists, flysch sediments); and (2) gneisses and micashists from the Briançonnais continent (Stutenbacker et al., 2018). The Helvetic nappes comprise mostly carbonates from a passive margin setting (Stutenbacker et al., 2018). Stutenbacker et al. (2018) modelled the relative importance of these three sources to sediment delivered to Lake Geneva through the analysis of sediment provenance. They estimated that 56.9% ± 9.6% of sediment comes from the External Massifs, 23.4% ± 2.3% from the Penninics and 19.7% ± 1.0% from the Helvetics, and also calculated these proportions for a site upstream of the Avançon confluence with the Rhône and upstream of the Grand Eau confluence of the Rhône. The Avançon is almost exclusively underlain by Helvetics high in CaO (Table 2). The Grande Eau contains Helvetics and Penninics (Table 2). The two Rhône sites are relatively similar despite tributary inputs because at this distance downstream the tributary areas, and hence sediment supply rates, are much lower than the main Rhône. Thus, the Avançon and the Grand Eau have very different sediment sources in geological terms as compared with the main Rhône itself.

	Avançon	Rhône at Avançon junction[1]	Grande Eau	Rhône at Grande Eau junction[1]
Penninics	Area: 0%	27%	68%	27%
External massifs	0%	55%	0%	57%
Helvetics	100%	18%	32%	16%
SiO_2	30.8%	58.6%	Not measured	56.0%
CaO	27.5%	12.2%	Not measured	11.4%

Table 2. Relative contribution of litho-tectonic units to the sediment at Avançon-Rhône and Grande Eau-Rhône confluences. (1) indicates data from calculations in Stutenbacker et al. (2018). SiO2 and CaO data are from Stutenbecker et al. (2018)

This study used these differences in sediment provenance to identify where sediment deposited in the tributary mouth bars is likely to originate. Bed sediment samples were collected at locations within the mouth bar as well as within the tributary and upstream of the junction in the main stem (Figure 4). During measurement, access allowed more sites to be sampled for the Grande Eau than for the Avançon. In order to validate our methods, we included three of the

sites measured by Stutenbacker et al. (2018): in the Rhône upstream of the Avançon and the Grande Eau respectively, and in the Avançon. Stutenbacker et al. did not measure the Grande Eau. At each sample location we sampled at a number of sediment depths.
The samples were prepared and crushed in the laboratory to obtain a homogenous dry powder which were then calcined and mixed with Lithium-Tetraborat powders. A total of 1.2g of these powders was used to prepare fused-disks for each sample. These disks were then analysed in the laboratory using X-ray florescence (XRF) spectrometry to identify and quantify their major chemical elements (SiO_2, TiO_2, Al_2O_3, Fe_2O_3, MnO, MgO, CaO, Na_2O, K_2O, P_2O_5, Cr_2O_3, NiO). XRF is capable of measuring elements in concentrations from ppm level up to 100wt% and of identifying high-SiO_2 and low-SiO_2 and carbonate rocks.

3 Results

3.1 Bed morphology and surface and near-bed planform velocities

Figure 8 shows the bathymetry and near surface and near bed velocity vectors, obtained for the Avançon–Rhône confluence with Mar=0.019. The bathymetry (Figure 8a) shows the presence of bed discordance with the tributary higher than the main channel. Because of this discordance, flow from the tributary enters the main channel only in the upper part of the water column and forces water at the surface towards the outer bank (Figure 8b). The main-channel flow is not influenced by the tributary in the lower part of the water column (Figure 8c), which implies a two-layer flow structure at the tributary mouth. The tributary mouth bar, which extends down the tributary side of the main Rhône, reduces the main channel width by almost 30% and leads to flow acceleration at both the surface (Figure 8a) and the bed (Figure 8b). At about 0.5 multiples of the main stem width downstream from the tributary, the apex of the tributary mouth bar has been passed and the main channel flow expands, even as it continues to accelerate. Near the bed (Figure 8c), there is also flow acceleration but both the tributary and the tributary mouth bar seem to have less effect upon the flow. The net result of the tributary and its mouth bar is curvature of the flow in the main channel. Whether due to flow acceleration (Figure 8b) or secondary circulation (see below) there is evidence of scour, displaced to the true left of the main Rhône (Figure 8a). The bridge had no piers, but it did narrow the channel very slightly (about 5%). As the Froude number during measurement was 0.56 it is unlikely that the measured flows are influenced by this.

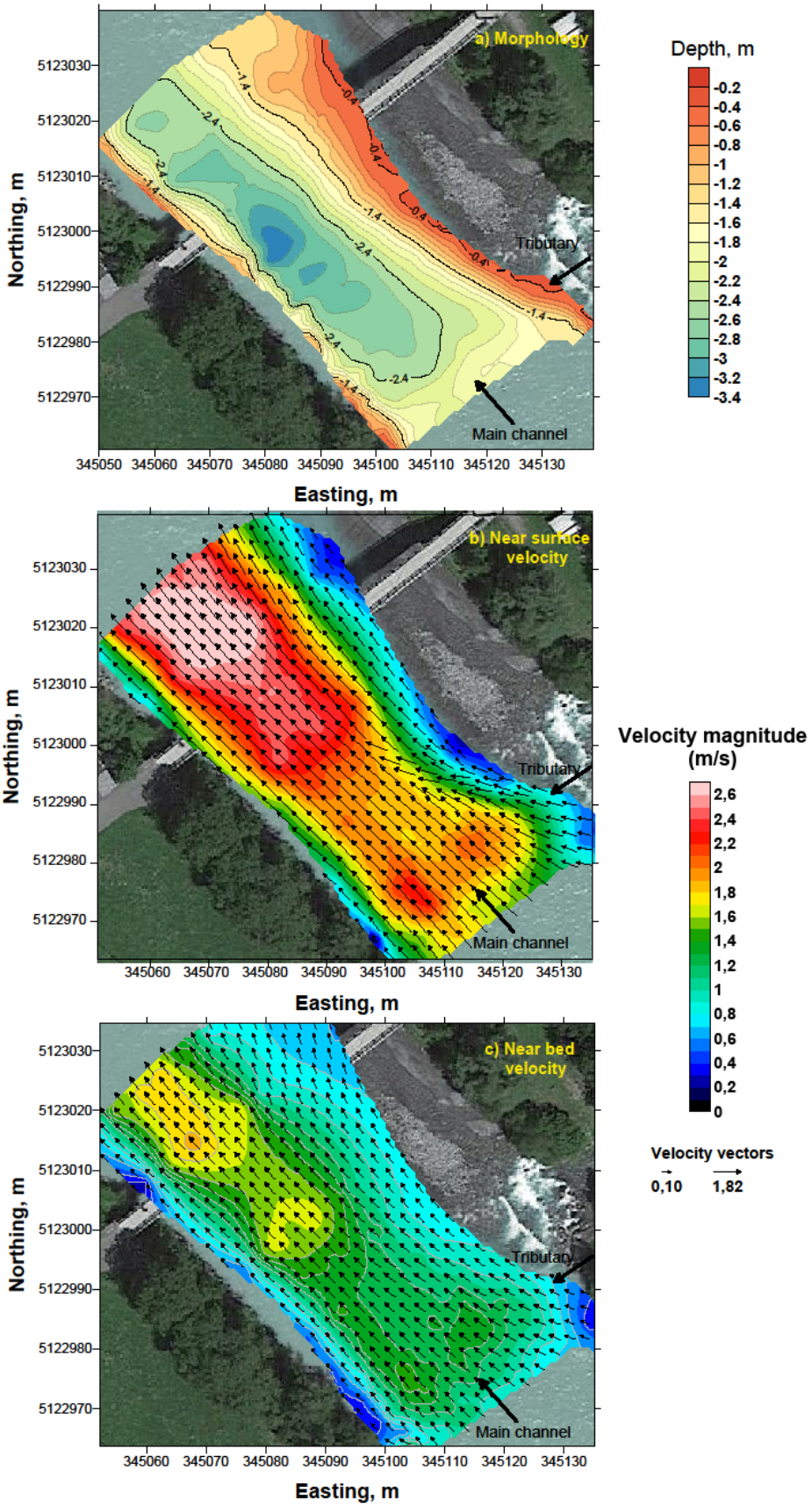

Figure 8. Avançon-Rhône confluence: patterns of morphological changes (a) and planform velocity vector distributions from moving ADCP measurement close to the free surface (b) and near the bed (c) and velocity magnitudes (contours in b & c).

The results obtained for Lizerne-Rhône confluence (Figure 9a) are different to those for the Avançon-Rhône. The bed is concordant, there is no tributary mouth bar and there is a scour hole near the inner bank (Figure 9a). The angular momentum ratio was slightly lower than the Avançon during measurement (0.015 rather than 0.019) but there is no evidence of tributary penetration into the main flow, at either the surface (Figure 9b) or the bed (Figure 9c), nor of flow acceleration or deceleration. The presence of the scour hole suggests that there are conditions that lead the tributary to have a morphodynamic impact upon the main channel bathymetry, but that the main river is able to preserve the associated scour hole once developed.

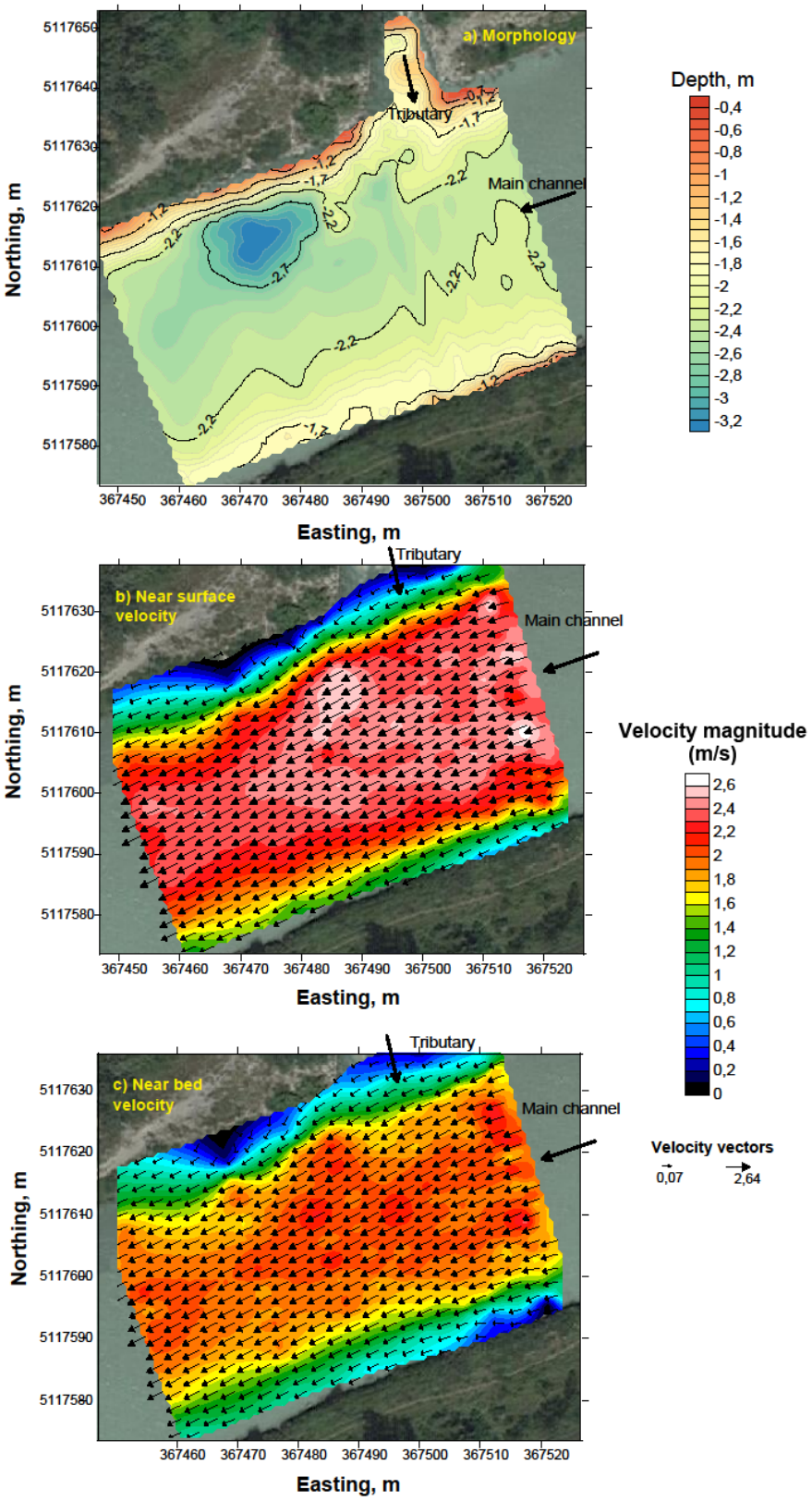

Figure 9. Lizerne-Rhône confluence: patterns of morphological changes (a) and depth-averaged streamwise velocity vector distributions from moving ADCP measurement close to the free surface (b) and near the bed (c) and velocity magnitudes (contours in b & c)

The Grand Eau-Rhône confluence has a discordant bed (Figure 10a) and the tributary meets the main stem flow in the upper part of the water column. There is some evidence of a scour hole but this is found more towards the centre of the main channel and downstream, as compared with the Avançon (Figure 10a). There is a tributary mouth bar, and this extends from about half way across the tributary and well down into the main channel (Figure 10a). The bar appears to have two distinct surfaces, at about 1 m depth starting at the tributary mouth, and then with a higher zone starting from Northing 5132305 m. The velocity vectors in Figure 10b suggest reduced penetration of the Grande Eau into the Rhône as compared with the Avançon, although there appears to be some surface flow deflection at the tributary mouth at the surface. Flow then returns to the right (i.e. tributary bank) before a second zone of deflection around the higher zone of the bar further downstream. There is evidence of flow constriction and acceleration of the surface flow (Figure 10b) but less so at the bed (Figure 10c).

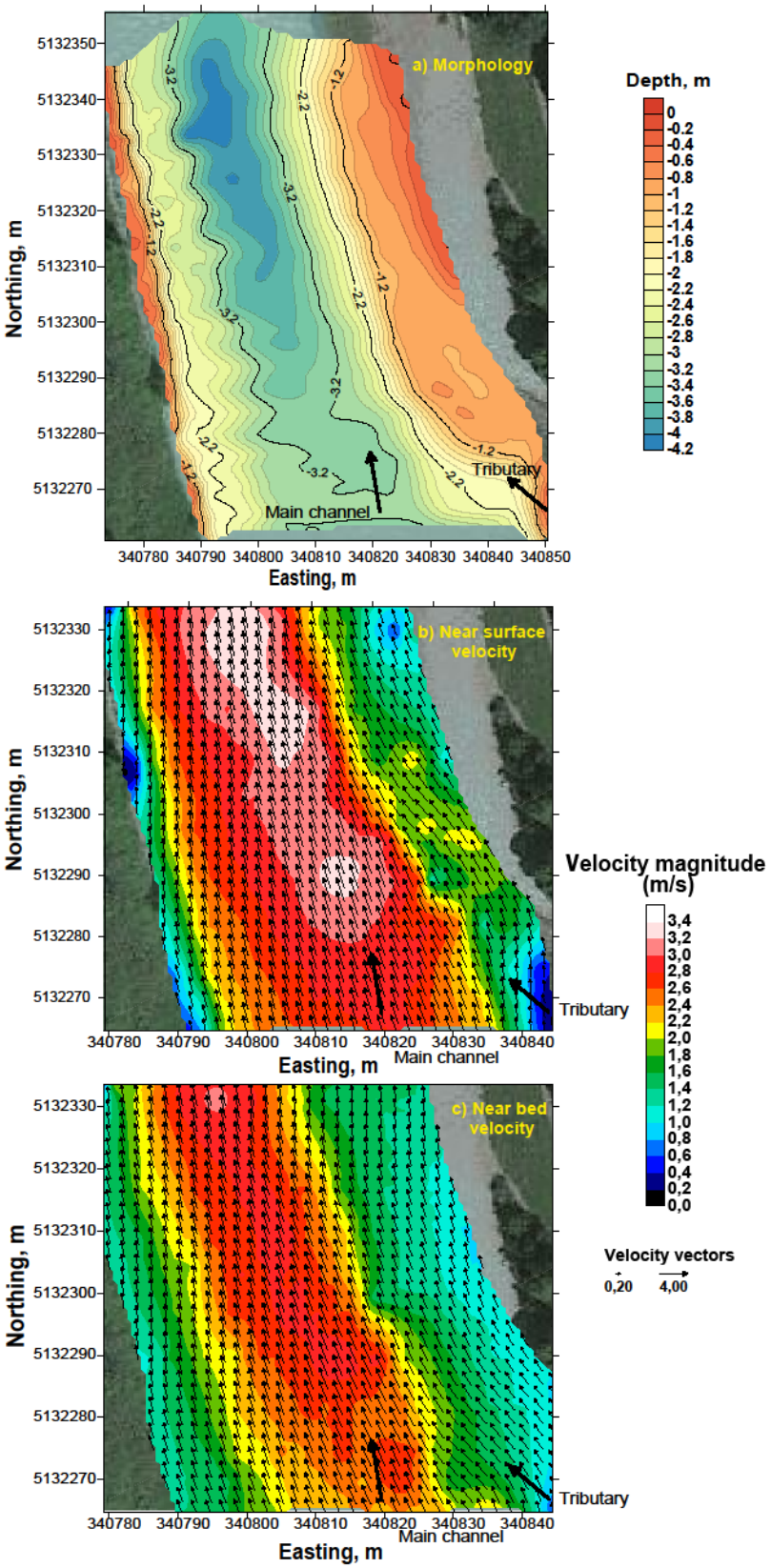

Figure 10. Grande Eau-Rhône confluence: patterns of morphological changes (a) and depth-averaged streamwise velocity vector distributions from moving ADCP measurement close to the free surface (b) and near the bed (c) and velocity magnitudes (contours in b & c)

3.2 Secondary flow velocities

Primary and secondary velocities were calculated for six cross sections at each confluence (cross-section locations were added as small sketches to Figures 11-13). Figure 11 shows these results for selected cross sections of the Avançon-Rhône confluence. At cross sections 1 and 3, flow originating from the tributary enters the main channel, with a downwelling motion towards the bed and flow that is directed towards the main channel throughout the flow depth (see the red boxes). At cross section 5 (see the red box), this flow behaviour continues near the bed, but is reduced in magnitude near the surface. At section 7 there is what corresponds to the downstream junction corner with a zone of very low magnitude velocity. To left of this zone, there is the continued presence of flow directed towards the true left. This is also present at section 9, but by section 11 there is flow directed towards the true right (Figure 11), at the downstream end of the bar (Figure 4a, Figure 8a).

These observations show clear tributary penetration into the main flow. However, this is superimposed on a second large-scale flow structure. Sections 1 and 3 in particular (Figure 11), also sections 5 and 7, show true right directed flow on the outer bank of the channel. When combined with the tributary penetration, they result in flow convergence in the middle of each section and downwelling, notably in Sections 1, 3 and 5. We attribute this to the channel narrowing and flow acceleration, aided by the tributary mouth bar that forms at and downstream of the Avançon. The downwelling seems to be displaced slightly to the true right side of the deepest part of each section (i.e. the zone of scour) perhaps suggesting that the scour forms during times when the tributary flow has a higher momentum and can penetrate more into the main flow; but that it can be maintained at lower momentum ratios.

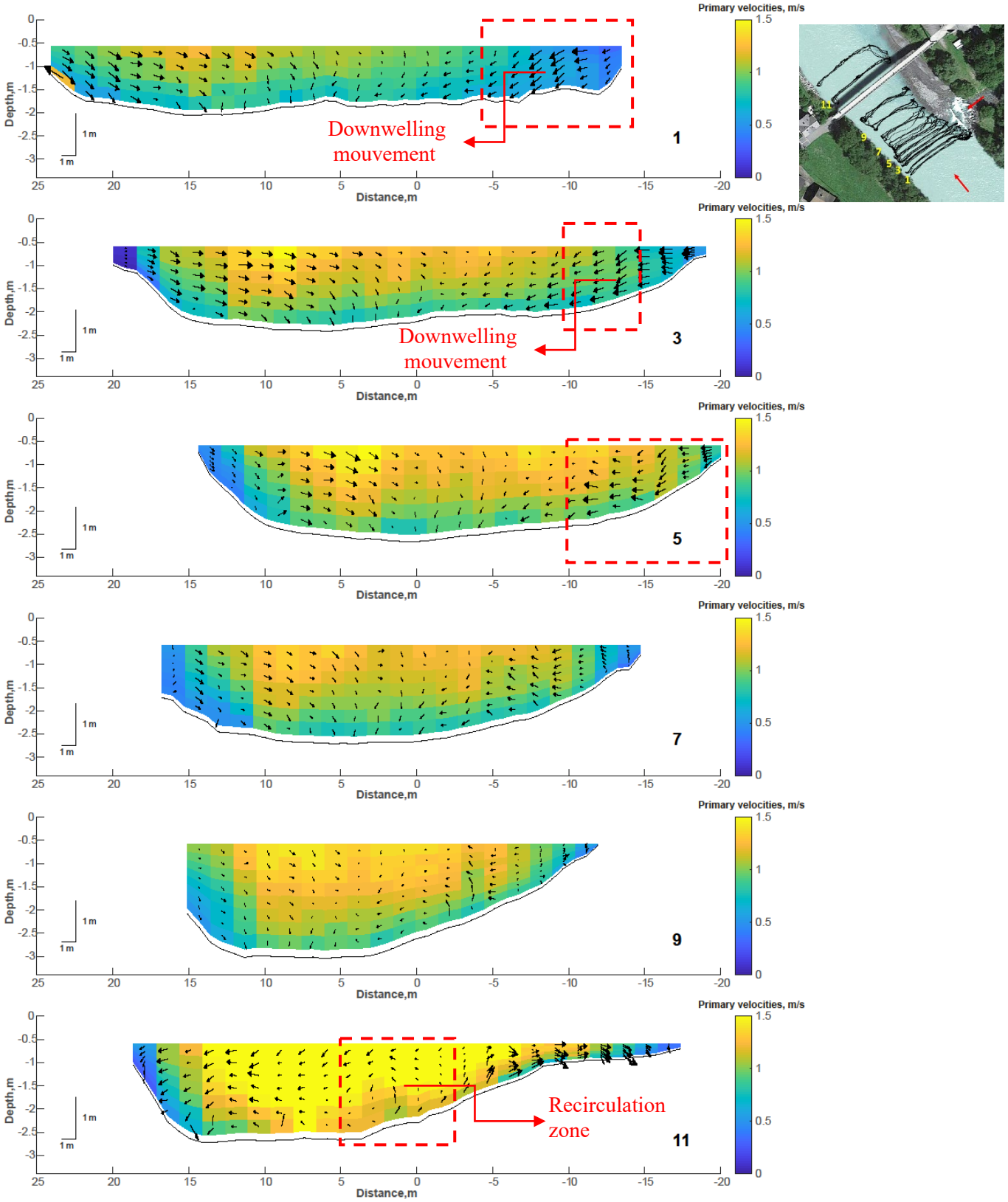

Figure 11. Avançon-Rhône confluence: cross-section lines 1,3,5,7,9 and 11 with primary velocity contours (m/s) and secondary velocity vectors (m/s). Right parts of the figures represent the tributary side of the main channel. 0 datums in x axes are the middle point of the cross section and positive and negative values show the distance of the middle cross section point from each bank.

Figure 12 shows primary and secondary velocities for selected cross sections at the Lizerne-Rhône confluence where the bed is concordant. Downstream of the junction apex, the flow patterns differ significantly from those observed at the Avançon-Rhône confluence with a discordant bed. The first thing that can be observed is that at cross-sections 3 and 5, the tributary enters the main channel with a much lower magnitude of the penetration. Still, this penetration is enough to push the mean Rhône flow toward the outer bank and to produce a large zone of low flow on the tributary side of the main channel. By section 7, as this penetration is weak, with the reduction of the flow curvature, the flow in the main channel reverses on the other side of the tributary.

This suggests that whilst the momentum ratio at Lizerne-Rhône confluence is similar to that of the Avançon-Rhône confluence, and both tributaries enter the main stem at 90 degrees, the systematic flow convergence and divergence that is apparent in the Avançon-Rhône confluence is not observed. The logical reason here could be the bed concordance at Lizerne-Rhône confluence which disturbs the tributary flow over a greater depth and reduces its ability to penetrate the main stem.

Finally, there are secondary motions in the main channel but these are less coherent and likely to be a product of main channel turbulence anisotropy.

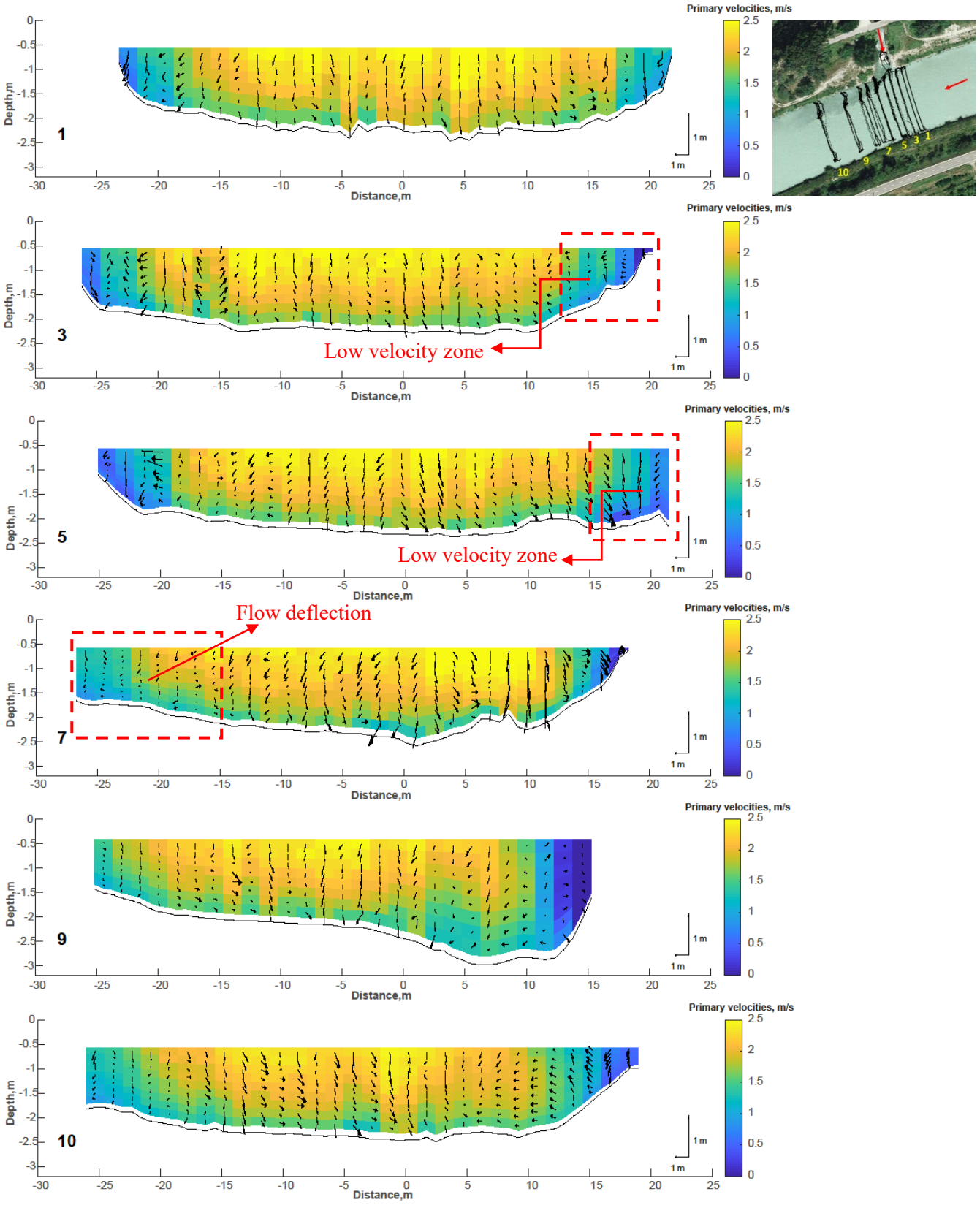

Figure 12. Lizerne-Rhône confluence: cross-section lines 1, 3,5,7,9 and 10 with primary velocity contours (m/s) and secondary velocity vectors (m/s). Right parts of the figures represent the inner bank. 0 datums in x axes are the middle point of the cross section and positive and negative values show the distance of the middle cross section point from each bank.

For the Grande Eau-Rhône confluence (Figure 13), for cross sections 1 and 3, there is very strong upwelling where the tributary joins the Rhône, into very slow velocity zones upstream and at the junction corner, which creates a small stagnation zone. Flow directed from the tributary into the main flow is not really apparent, and this may reflect the much lower junction angle. Tributary penetration is clear at section 5, the section that corresponds to the downstream junction corner and this continues at section 8. By section 8, a very weak circulation cell has developed (-14 to -20 m laterally), and this seems to be present at sections 9 and 11.

As with the Avançon, there is strong flow directed towards the true right on the outer bank of the channel, from section 3 through to section 9, as the flow accelerates. The result is flow convergence, with some evidence of flow convergence and downwelling at sections 5 and 8 (Figure 13). As with the Avançon, this downwelling is slightly displaced to the true right of the scour hole. In this example, even though the tributary penetration seems to be reduced, the presence of the bank attached tributary mouth bar seems to reduce channel width by almost 20%, causes flow acceleration and in turn causes the formation of channel scale secondary circulation.

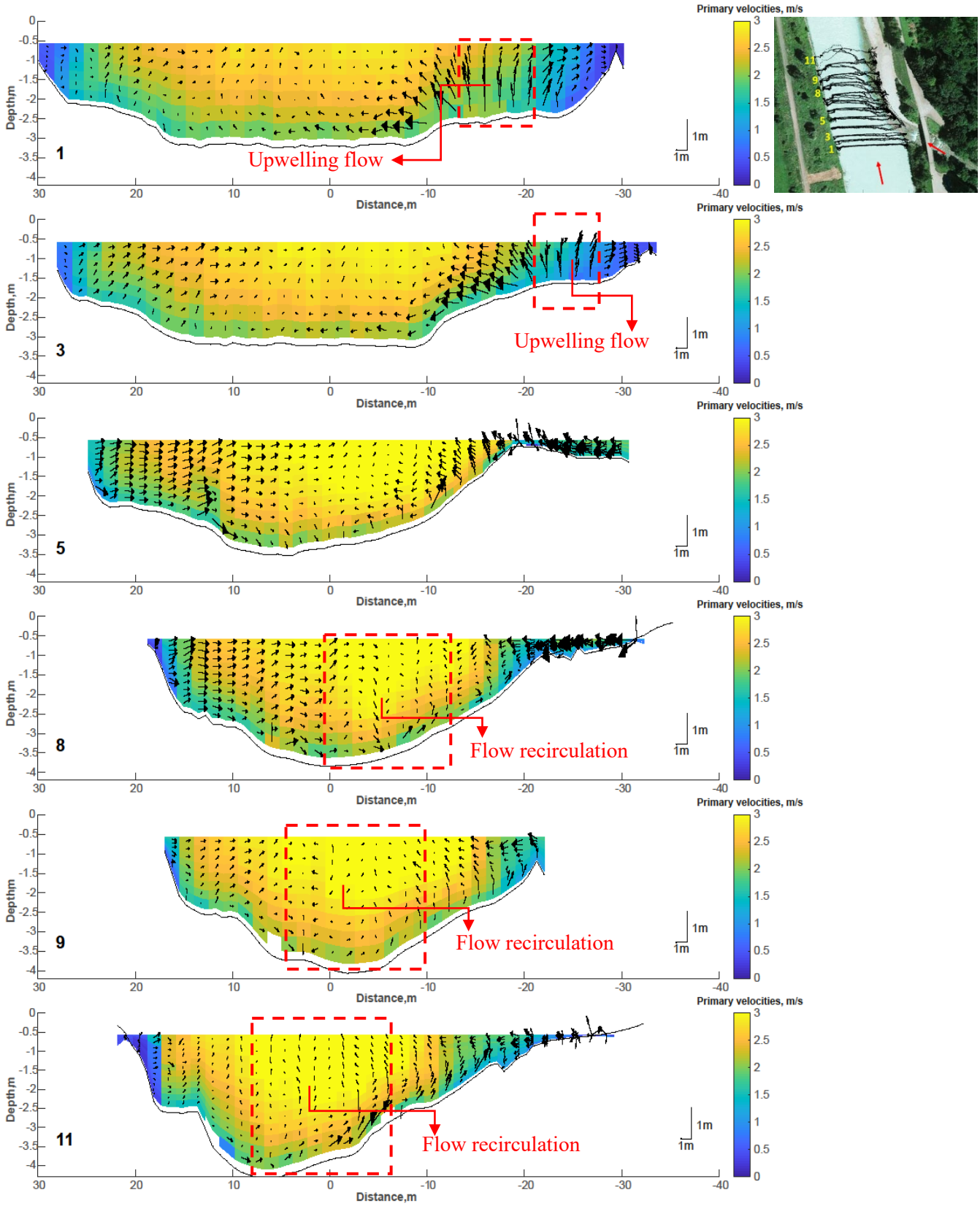

Figure 13. The Grande Eau-Rhône confluence: cross-section lines 1, 3,5,8,9 and 11 with primary velocity contours (m/s) and secondary velocity vectors (m/s). Right parts of the figures represent the tributary side of the main channel. 0 datums in x axes are the middle point of the

cross section and positive and negative values show the distance of the middle cross section point from each bank.

3.3 Angular momentum ratio

Table 1 included estimates of the angular momentum ratio for all three confluences. That for the Avançon-Rhône confluence is the highest and would support penetration of the tributary into the main channel being the highest as well. This value is lower for the Grande Eau-Rhône confluence, despite the latter having a higher momentum ratio without correction for angular effects, suggesting there should be less penetration of the Grande Eau into the Rhône. For the Lizerne-Rhône confluence this value is the lowest which suggests there should be a lower penetration of the tributary into the main stem. It might be expected that as angular momentum increases, the likelihood of two-phase flow increases because it is more likely the tributary has sufficient momentum to penetrate over the main channel flow. This is a hypothesis that merits further evaluation, likely using numerical models.

3.4 Tributary mouth bar mineralogy

Table 3 shows the validation of the provenance analyses. It confirms a good agreement for the surface samples between the data of Stutenbacker et al. (2018) and the data used in this study, perhaps less so for the proportion of CaO for the tributary sample in the Avançon. The results also show that sediment in the Avançon tributary and in the Grande Eau surface samples have elevated CaO and reduced SiO_2 as compared with the main Rhône such that we can use the CaO and SiO_2 composition in the tributary mouth bar to indicate its likely provenance. We were also able to access the Avançon tributary to do some samples at depth; this was not possible in the Grande Eau due to the flow magnitude. The results are interesting as they show that with depth the CaO concentration rises whilst the SiO_2 concentration falls, implying that deeper in the tributary bed sediments the provenance becomes more typical of Helvetics. We suggest that this reflects occasional penetration into the tributary of Rhône water and fine sediment at particular low momentum ratios.

Site	This study: SiO_2	This study: CaO	Stutenbacker et al. (2018) SiO_2	Stutenbacker et al. (2018) CaO
Rhône upstream of Avançon (surface)	61.3%	10.6%	58.6%	12.2%
Rhône upstream of Avançon (0.23 m depth)	59.2%	12.3%	X	X
Rhône upstream of Avançon (0.44 m depth)	61.4%	11.2%	X	X
Avançon trib. (surface)	45.3%	28.5%	42.3%	37.8%
Avançon trib. (0.17 m depth)	37.1%	42.8%	X	X
Avançon trib. (0.26 m depth)	20.0%	67.8%	X	X
Avançon trib. (0.37 m depth)	17.0%	71.7%	X	X
Rhône upstream of Grande Eau (surface)	53.0%	15.1%	56.0%	11.0%
Grande Eau trib. (surface)	30.8%	30.3%	X	X

Table 3. Comparison of Stutenbacker et al. (2018) data (% by weight) with data acquired in this study for sites upstream of the Avançon and Grande Eau junctions on the Rhône and in each tributary.

Figure 14 shows data for the three locations sampled in the Avançon- Rhône confluence plotted against their absolute elevation. The sediment near the surface of the bar (sample A in Figure 4a) has more CaO than SiO_2. There are two samples at comparable elevations to samples in the Avançon tributary. For both, proportions of bar and tributary samples are similar. However, the bottom two bar samples show much higher SiO_2 and lower CaO proportions, suggesting that lower in the bar, there is greater mixing in of sediment derived from the Rhône; the base of the bar is formed partly from main channel sediments.

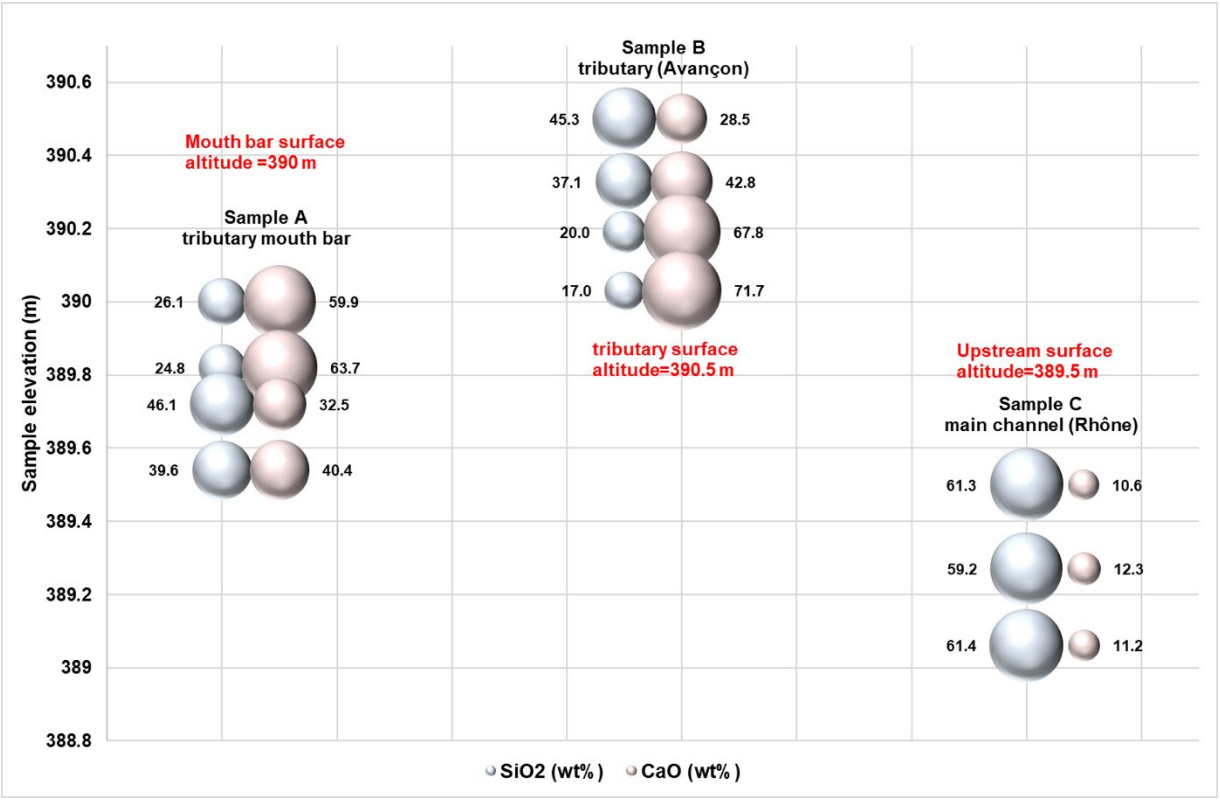

Figure 14. Mineralogical provenance of the collected samples shown as proportional circles. Blue circles show the amount of SiO_2 and pink circles show the amount of CaO for the collected samples at Avançon-Rhône confluence

Samples in the Grande Eau-Rhône confluence are different. On the bar, samples (locations A-F in Figure 4c) contain only a modest amount of SiO_2, with almost all samples at all depths dominated by CaO (Figure 15). The tributary sediment (sample I) is also mostly CaO, whereas the main channel sediment (sample H) is mostly SiO_2. These data suggest that even at depth, sediment in the bar is mainly sourced from the Grande Eau. The junction angle is much smaller and it is probable that the Grande Eau can more readily steer its sediment into the zone of bar formation. It is possible that right at the most downstream sampled location there is some main channel sediment deposition (sample F), where a higher percentage of SiO_2 was observed near the surface, which could reflect finer sediment deposition of main channel derived sediment within the post-confluence zone. It is also possible that the fine sediments deposited at the downstream end of the bar are related to confluence hydrodynamics during bar formation in higher flow events. For instance, upwelling of fine sediment at the downstream end of the bar could be attributable to either: 1) the kinds of secondary circulation identified by Rhoads et al. (2009); or 2) to the development of a two-layer flow structure (Leite Ribeiro et al., 2012), where the flow from the main channel moves over the tributary flow and delivers sediment to the downstream end of the bar. We do not have data that could confirm either of these hypotheses.

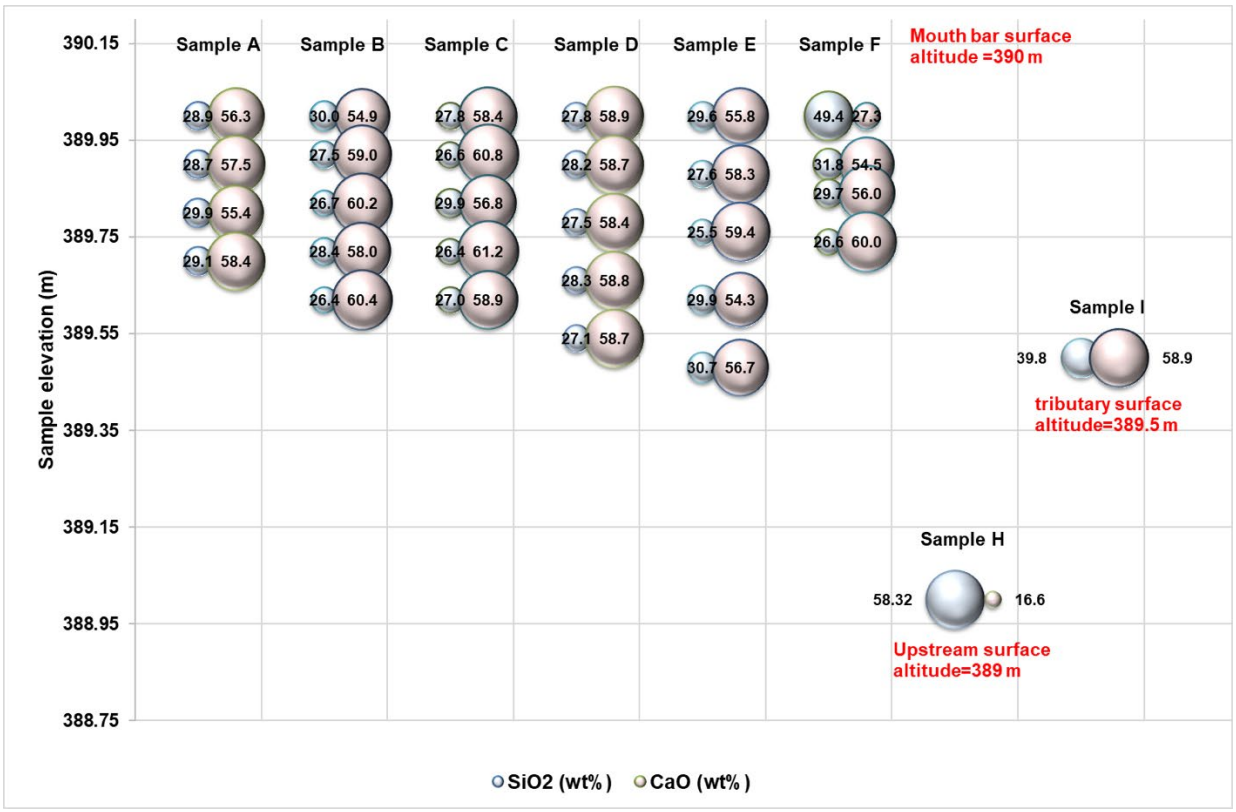

Figure 15. Mineralogical provenance of the collected samples shown as proportional circles. Blue circles show amount of SiO_2 and pink circles show the amount of CaO for the collected samples at Grande Eau-Rhône confluence

4 Discussion

The results of this study reveal the complex flow behaviour and morphological changes in three confluences with very low momentum ratios during measurement but very different junction angles and long-term rates of sediment supply. In this section we discuss the similarities and differences in flow structure and morphological aspects of these three confluences as compared to previous conceptual models of river channels with different characteristics, proposed by Best (1987,1988), Mosely (1976) and Leite Ribeire et al. (2012). Overall, the general flow and morphological patterns are highly influenced by the junction angle and sediment supply.

4.1 Sediment transport rate

As there was no sediment transport in the tributary during measurement, transport rates for tributary sediment transporting events were not estimated because sediment transport capacity calculations suggest errors across 5 orders of magnitude for this kind of river (Antoniazza et al., 2022) but also because sediment transport is strongly influenced by changes in sediment supply. Comparison of two case studies with different tributary sourced sediment supply (Avançon-Rhône confluence and Lizerne-Rhône confluence) suggests that if the tributary is able to supply significant sediment supply (as at the Avançon-Rhône confluence) the formation of a pronounced bed discordance and tributary mouth bar is possible. The effect of bed discordance on flow dynamics and bed morphology has been reported by Biron et al. (1996a, 1996b), Best and Rhoads (2008), Djordjevic (2008) and Leite Ribeiro et al. (2012). Leite Ribeiro et al. (2012) were the first to draw attention to the potentially modifying effect of tributary sediment delivery, by studying the junction morphology that formed where the tributary had a low flow momentum compared to the main channel.

In the experiments of Leite Ribeiro et al. (2012) and Guillén Ludena et al. (2015, 2016), the discharge in the tributary and the main stem were applied to sediment transport formulae to set sediment supply rates. Their experiments were performed in the laboratory with a constant sediment discharge, which was supplied to the tributary and the main channel. They also discussed the formation of the two-layer flow associated with the bed discordance. In field cases, it is likely that the tributary supplies sediment at different times (and with different calibre) to the main channel because of different distances between the confluence and potential sediment sources and different hydrological regimes.

In low momentum ratio river confluences, if the sediment supply from the tributary is high enough, the low momentum does not result in particularly strong jet formation (Figure 11) and the tributary flow seems to be rapidly-steered, even at the surface (Figure 8). However, it is clear that the tributary mouth bar extends downstream from the downstream junction corner (Figure 8) with a sustained narrowing of the main channel and flow acceleration (Figure 8). There is the appearance of a scour hole, flow convergence and some flow downwelling (Figure 11). This is likely to reflect the combined effects of tributary penetration and bar driven main channel narrowing. A slight displacement of the downwelling to the tributary side of the scour hole suggests that the scour hole may have formed when the tributary momentum was higher, which would increase flow acceleration, downwelling and hence erosion. The tributary mouth-bar that extends along the inner bank of the main channel is related either to the low flow velocity zone or to the flow recirculation zone, which favour sediment deposition therein. Most of the sediment that form this bar could be a result of the sediment deposition sourced from the tributary.

Biron et al. (1993) discussed the absence of marked scour holes at discordant confluences. Guillén Ludeña et al., (2015) observed a deeper scour hole at the outer bank of the main channel and a narrower and higher bank-attached bar at the inner bank as discussed above. It is likely that these differences relate to tributary sediment supply differences. These differences could also be related to the confluence configuration for each case; rigid lateral banks in the case of Guillen-Ludeña et al. (2015); and erodible banks in the case of Biron et al. (1993). The discharge ratio may also play a role in these differences. Where tributary sediment supply is higher and a tributary mouth bar can form and attach itself to the bank downstream of the tributary, channel cross-section area is reduced, flow is accelerated and converges, and the combined flow acceleration and downwelling flow which could be the result of either secondary circulation or bed discordance (there is no data available for this study to confirm the mechanism). Intriguingly, the sediment provenance studies suggest that the tributary mouth bar relates to sediment sourced from both the tributary and the main channel because the sediments originating from the main channel may have been transported there by flow upwelling or by secondary currents (Rhoads, 2009). Observations suggest that tributary mouth bars can be periodically trimmed and eroded by the main channel, to leave a more classical discordant confluence (Moesly,1976), with weaker tributary mouth bar penetration, more typical of what was observed by Biron et al. (1993). In such situations, as sediment supply in the main channel or the tributary increases, sediment from the main channel is likely to move underneath the tributary explaining why more Rhône sediment than expected was found at the base of the Avançon tributary mouth bar; the sediments originating from the main channel may have been transported there by flow upwelling or by secondary currents (Rhoads, 2009). Further fieldwork or computational modelling is needed to assess this effect.

On the other hand, if the tributary sediment supply is not significant (Lizerne-Rhône confluence), the bed is concordant. For the same momentum ratio, this reduces tributary penetration. A weak mixing interface moves toward the inner bank farther downstream and

prevents the formation of the downstream attached bar at this bank, even with sediment provided by the main river, in the absence of tributary sediment supply. There is perhaps some evidence of scour in this zone, attached to the tributary side of the channel (Figure 9).

Comparing the Avançon confluence and the Lizerne confluence, which have the same junction angle and very similar momentum ratios at the time of measurement, but very different sediment supply rates, it is apparent that markedly different bathymetries and flow structures form. In forming a tributary mouth bar that may then become attached to the downstream true inner bank, tributary sourced sediment can lead to substantial impacts on the main channel flow, even at very low flow momentum ratios and when the tributary is no longer actively supplying sediment. This is a legacy effect with the bar forming at times when the tributary momentum is likely to have been higher (i.e. when it is capable of delivering sediment) and that lasts as long as the main channel is unable to erode the bar that forms.

4.2 Junction angle and angular momentum ratio

The junction angle controls the curvature of merging flows, and the comparison of the Avançon (higher junction angle) and Grande Eau (lower junction angle) suggest that lower junction angle but high tributary sediment supply will modify bathymetry in degree rather than in kind. Previous laboratory and field studies have shown that increasing the junction angle enhances the curvature of the merging flow and facilitates the penetration of the tributary flow into the main channel (Best, 1988; Rhoads & Kenworthy,1995; Rhoads & Sukhodolov, 2001). Our results support these conclusions, in that the Avançon (with higher junction angle) penetrated into the Rhone more than the Grande Eau (with lower junction angle); and this effect was captured by correcting the momentum ratios for angular effects. Both confluences have discordance and were measured at similar momentum ratios, and so the formation of a relatively weak jet-like tributary flow at the Avançon is likely to be a result of a greater junction angle. This is the classic two-layer flow proposed by Leite Ribeiro et al. (2012). This two-layer flow was not observed at the Grande Eau, possibly because of a lower junction angle which leads to a lower angular momentum ratio and thus less penetration of tributary flow into the main channel. One might expect a greater likelihood for two-layer flow as angular momentum ratio increases because the tributary will have greater momentum to penetrate over the main channel flow. This hypothesis could be assessed in future work, perhaps with the aid of numerical modelling. On the other hand, although difficult to detect conclusively in the data, a zone of stagnation was found at Grande Eau upstream of the junction throughout the flow depth, and a stagnation is more likely to occur if there is two-layer flow because the penetrating tributary flow creates a barrier.

Given that both the Avançon and Grande Eau delivered sediment to the Rhone, our results allow evaluation of the influence of junction angle for tributaries with sediment supply. Junction angle appears to modify the effects of tributary sediment delivery. The tributary mouth bar that formed at the Grande Eau contained less main river sediment and was dominated by sediment supplied from the tributary. The reduced junction angle at the Grande Eau appears to have facilitated the re-orientation of tributary supplied coarse sediment, forming the downstream attached bar, with tributary supplied sediment throughout its depth. This is field confirmation of the laboratory observations of Guillén-Ludeña et al (2016). The bed discordance at the Avançon-Rhône confluence and a higher junction angle lead to a greater penetration of the tributary into the main channel. It may also encourage formation of a larger recirculation zone downstream of the junction, which perhaps allows main channel sediment to recirculate onto the bar, particularly during conditions of low tributary flow. That could be the reason why the mouth bar is formed with both tributary and mainstream sediment.

4.3 Hydrodynamics

Mosley (1976) and Best (1987, 1988) showed that at momentum ratios close to one and for channels that both turn through the same angle, two helical cells form downstream of the junction, close to the confluence, within the near-field region defined as the confluence hydrodynamic zone (e.g. Konsoer and Rhoads, 2014). Mosley (1976) showed that where the momentum ratio is near one, these helical cells are well-developed counter-rotating and occupy equal proportions of the main channel cross section. By increasing the momentum ratio, the tributary adjacent cell starts to prevail and occupies a greater proportion of the channel cross-section. Mosley also showed that for momentum ratios less than one, the penetration of the flow originating from the tributary into the main channel reduces (see also Rhoads and Johnson, 2018) and the position of the mixing interface migrates towards the tributary. With very low M_r (e.g. Riley and Rhoads (2012) report data for M_r=0.27) there may be no tributary side secondary circulation cell. Results obtained for Lizerne-Rhône confluence are in good agreement with these previous findings. For both the Avançon and the Grande-Eau confluences, significant secondary circulation was found even at very low momentum ratios, and it is logical to conclude that what makes these cases different to the more general model is the presence of high rates of coarse sediment supply and tributary mouth bar formation and discordance, expected for tributaries draining mountain zones. Such effects are likely to be modified by junction angle. In turn, this finding suggests that momentum ratio on its own cannot be used to generalise the morphodynamics of confluences: how the momentum is distributed with respect to the main channel (i.e. a discordance index) as well as modification of the momentum ratio to become an angular momentum ratio is needed.

It is the tributary with the lowest angular momentum that is likely to penetrate least into the confluence. This may reduce to below one for the momentum ratio at which both the main stem and tributary have a significant influence on the confluence flow field. As the momentum ratio falls further, the tributary influence should progressively decline. It then may be necessary to have angular momentum ratios for both the concordant and the discordant case to capture tributary sediment delivery effects.

4.4 Conceptual Model for Low Momentum Ratio Confluences

The evidence obtained from this study shows that none of the existing conceptual models can fully explain the flow behaviour in confluences with low momentum ratio. Although Boyer et al., (2006) has reported conceptual models for M_r<1, their conceptual model is limited to high flow conditions where there is the presence of bed discordance. They also reported the absence of the scour hole at the outer bank. Leite Ribeiro et al., (2012) and Guillén Ludeña et al., (2015, 2016, 2017) studied river confluences with low momentum ratio, however their models were limited to a specific case of river confluences with high and equivalent rates of sediment delivery from the tributary and the main channel. Their studies also were limited to discordant confluences with large junction angles. Best (1988) investigated asymmetric confluences with concordant beds, in a small laboratory flume and Leite Ribeiro et al., (2012) showed important differences between this conceptual model and confluences with low momentum ratio and high rates of sediment delivery, such as found in mountainous regions.

With regard to the above discussion, Figure 16 shows a proposed conceptual framework for river confluences characterized with very low momentum ratio and various rates of sediment supply from the tributary into the main channel. As shown in Figure 16A, in the presence of a significant discordance at the mouth of the tributary, due to the high sediment supply originating from the tributary, the scour hole is shifted from the confluence zone toward the outer bank. High tributary sediment supply forms a mouth bar and this may extend downstream attached to the tributary side of the bank. This bar may develop from deposition of main channel sediment

as well as tributary sediment. There is no evidence for the active sediment transport in this case because the tributary flow is not competent enough to supply a high amount of sediment all the time, but in high sediment transport periods, due to the presence of the two layer flow which results in the formation of the secondary circulation, sediment from the main channel could move under that of the tributary and the bar could be vertically developed by the deposition of the tributary sediment. Decreasing the junction angle (Figure 16C) means the reduction of the angular momentum ratio and the penetration of the tributary flow into the main channel; results in a scour hole more towards the middle of the main channel; and is associated with a bar along the tributary side bank of the main channel, downstream of the confluence. This bar develops due to deposition of primarily tributary sediment because the tributary is better able to steer the sediment to orient itself parallel to the main flow and develop the bar more laterally than the Avançon confluence. In the case where the sediment transported from the tributary into the main channel is not significant or the dominant sediment supply originates from the main channel (Figure 16B), no bed discordance develops, the scour occurs near the inner bank, and the formation of the mouth bar is absent.

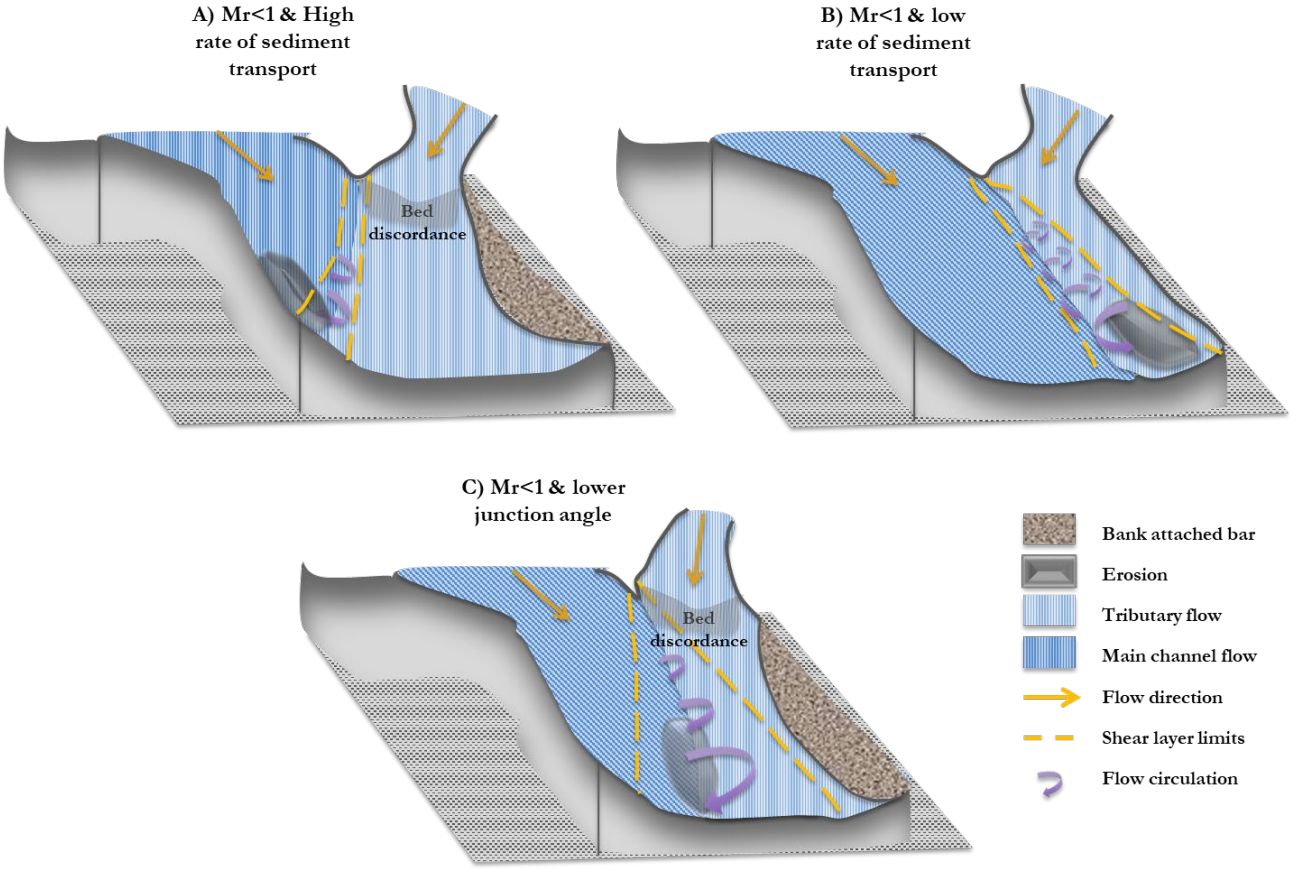

Figure 16. Proposed conceptual model for A) Mr<1 and high rate of sediment transport, B) Mr<1 and low rate of sediment transport and C) Mr<1 and high rate of sediment transport and lower junction angle (Boyer et al. 2006)

5 Conclusion

The present study based on field data at three medium sized confluences with low momentum ratio show that the tributaries which carry a significant amount of sediment into the main channel, have hydrodynamics and morphodynamics patterns which differ from classical models. They are often associated with a discordant bed. A downstream attached bar and a pronounced scour hole can also be observed, the latter reflecting the effects of bar formation on channel capacity and flow acceleration, convergence and downwelling. The result is that even at very low momentum ratios it is possible to have significant secondary circulation in the main

channel due to the legacy of previously delivered and deposited sediment as a tributary mouth bar.
Results indicate that the downstream bar can have different sediment origins, according to the angle of the junction. If the junction angle is lower, this bar can be a result of the tributary sediment supply. By increasing the junction angle, as the curvature of the merging flow is also increased, a jet may form, allowing main channel sediment to penetrate under the tributary inflow and accumulate at the base of the bar, as was measured in this study.

The results of the present study also demonstrate that at low momentum ratio confluences where the tributary supplies less sediment into the main channel, the tributary mouth bar does not form and it is even possible for a scour hole to form where a bar would be deposited in situations where the tributary delivers sediment. We attribute this to the reduced penetration of the tributary, leaving mixing closer to the tributary side of the channel.

As the results of the present study are limited to a small range of confluences with low momentum ratio and specific confluence configurations, further work is needed to determine how variations in other factors controlling flow pattern at confluences, such as the discharge ratio, junction angle, confluence planform symmetry, and variations in sediment transport rate, interact with hydrodynamics and morphodynamics of mountain river confluences. What this study has shown is that the sediment transport rate, discordance and angular momentum should be considered when defining the low momentum ratio river confluences and evaluating confluence hydrodynamics and morphodynamics.

Acknowledgements

The work was supported by Swiss National Science Foundation Grant 200021_160020. The data have been uploaded and archived in a PANGAEA repository at https://issues.pangaea.de/browse/PDI-21636.

References

Ashmore, P., Parker, G., 1983. Confluence scour in coarse braided streams. Water Resour. Res. 19, 392–402.

Ashmore, P.E., Ferguson, R.I., Prestegaard, K.L., Ashworth, P.J., Paola, C., 1992. Secondary flow in anabranch confluences of a braided, gravel-bed stream. EARTH Surf. Process. LANDFORMS 17, 299–311.

Antoniazza G., Nicollier T., Boss S., Mettra F., Badoux A., Schaefli B., Rickenmann D., Lane S. N., 2022. Hydrological drivers of bedload transport in an Alpine watershed. Water Resources Research. Peer-reviewed.

Best, J.L., 1987. Flow dynamics at river channel confluences: Implications for sediment transport and bed morphology. Recent Dev. Fluv. Sedimentol. Spec. Publ. SEPM Soc. Sediment. Geol. 27–35. https://doi.org/10.2110/pec.87.39.0027

Best, J.L., 1988. Sediment transport and bed morphology at river channel confluences. Sedimentology 35, 481–498. https://doi.org/10.1111/j.1365-3091.1988.tb00999.x

Biron, P., Best, J.L., Roy, A.G., 1996a. Effects of Bed Discordance on Flow Dynamics at Open Channel Confluences. J. Hydraul. Eng. 122, 676–682. https://doi.org/10.1061/(ASCE)0733-9429(1996)122:12(676)

Biron, P.M., Roy, A.G., Best, J.L., 1996b. Turbulent flow structure at concordant and discordant open-channel confluences. Exp. Fluids 21, 437–446. https://doi.org/10.1007/BF00189046

Boyer, C., Roy, A.G., Best, J.L., 2006. Dynamics of a river channel confluence with discordant beds: Flow turbulence, bed load sediment transport, and bed morphology. J. Geophys. Res. Earth Surf. 111, 1–22. https://doi.org/10.1029/2005JF000458

Bradbrook, K.F., Lane, S.N., Richards, K.S., Biron, P.M., Roy, A.G., 2001. Role of Bed Discordance at Asymmetrical River Confluences. J. Hydraul. Eng. https://doi.org/10.1061/(ASCE)0733-9429(2001)127:5(351)

De Serres, B., Roy, A.G., Biron, P.M., Best, J.L., 1999. Three-dimensional structure of flow at a confluence of river channels with discordant beds. Geomorphology 26, 313–335. https://doi.org/10.1016/S0169-555X(98)00064-6

Dietrich, W. E., and Smith, J. D., 1983. Influence of the point bar on flow through curved channels, Water Resources Research, 19, 1173– 1192. http://doi.org/ 10.1029/WR019i005p01173

Dinehart, R.L., Burau, J.R., 2005. Averaged indicators of secondary flow in repeated acoustic Doppler current profiler crossings of bends. Water Resour. Res. 41, 1–18. https://doi.org/10.1029/2005WR004050

Djordjevic, D. Numerical study of 3D flow at right-angled confluences with and without upstream planform curvature. J. Hydroinform. 2013, 15, 1073–1088.

Gartner, J.W., 2004. Estimating suspended solids concentrations from backscatter intensity measured by acoustic Doppler current profiler in San Francisco Bay, California. Mar. Geol. 211, 169–187. https://doi.org/10.1016/j.margeo.2004.07.001

Guillén-Ludeña, S., 2015. Hydro-morphodynamics of open-channel confluences with low discharge ratio and dominant tributary sediment supply. Ec. Polytech. Fédérale Lausanne, Switz. 6716. https://doi.org/10.5075/epfl-thesis-6716

Guillén-Ludeña, S., Franca, M.J., Cardoso, A.H., Schleiss, A.J., 2015. Hydro-morphodynamic evolution in a 90° movable bed discordant confluence with low discharge ratio. Earth Surf. Process. Landforms 40, 1927–1938. https://doi.org/10.1002/esp.3770

Guillén-Ludeña, S., Franca, M.J., Cardoso, A.H., Schleiss, A.J., 2016. Evolution of the hydromorphodynamics of mountain river confluences for varying discharge ratios and junction angles. Geomorphology 255, 1–15. https://doi.org/10.1016/j.geomorph.2015.12.006

Guillén Ludeña, S., Cheng, Z., Constantinescu, G., Franca, M.J., 2017. Hydrodynamics of mountain-river confluences and its relationship to sediment transport. J. Geophys. Res. Earth Surf. 122, 901–924. https://doi.org/10.1002/2016JF004122

Gunawan, B., Sterling, M., Knight, D.W., 2010. Using an acoustic Doppler current profiler in a small river. Water Environ. J. 24, 147–158. https://doi.org/10.1111/j.1747-6593.2009.00170.x

Hauet, A., Muste, M., H-C., H., 2009. High spatial resolution data acquisition for the geosciences: kite aerial photography. Earth Surf. Process. Landforms 34, 242–252. https://doi.org/10.1002/esp

Kostaschuk, R., Best, J., Villard, P., Peakall, J., Franklin, M., 2005. Measuring flow velocity and sediment transport with an acoustic Doppler current profiler. Geomorphology 68, 25–37. https://doi.org/10.1016/j.geomorph.2004.07.012

Kenworthy, S.T., Rhoads, B.L., 1995. Hydrologic control of spatial patterns of suspended sediment concentration at a stream confluence. J. Hydrol. 168, 251–263. https://doi.org/10.1016/0022-1694(94)02644-Q

Konsoer, K.M., Rhoads, B.L., 2014. Spatial–temporal structure of mixing interface turbulence at two large river confluences. Environ. Fluid Mech. 14, 1043–1070. https://doi.org/10.1007/s10652-013-9304-5

Lane, S.N., Parsons, D.R., Best, J.L., Orfeo, O., Kostaschuk, R. a., Hardy, R.J., 2008. Causes of rapid mixing at a junction of two large rivers: Río Paraná and Río Paraguay, Argentina. J. Geophys. Res. Earth Surf. 113, 1–16. https://doi.org/10.1029/2006JF000745

Leite Ribeiro, M., 2011. Influence of Tributary Widening on Confluence Morphodynamics. Ec. Polytech. Fédérale Lausanne, Lausanne, Switz. https://doi.org/10.5075/epfl-thesis-4951

Leite Ribeiro, M., Blanckaert, K., Roy, A.G., Schleiss, A.J., 2012. Flow and sediment dynamics in channel confluences. J. Geophys. Res. Earth Surf. 117. https://doi.org/10.1029/2011JF002171

Lewis, Q.W., Rhoads, B.L., 2015. Rates and patterns of thermal mixing at a small stream confluence under variable incoming flow conditions. Hydrol. Process. 29, 4442–4456. https://doi.org/10.1002/hyp.10496

Li, K., Yuan, S., Tang, H., Xiao, Y., Xu, L., Huang, S.,Rennie, C.D., Gualtieri, C.A. Field study of near-junction-apex flow at a large river confluence and its response to the effects of floodplain flow. J. Hydrology, 610:127983,2022.

Moradi, G., Vermeulen, B., Rennie, C.D., Cardot, R., Lane, S.N., 2019. Evaluation of aDcp processing options for secondary flow identification at river junctions. Earth Surf. Process. Landforms. https://doi.org/10.1002/esp.4719

Mosley, M.P., 1976. An Experimental Study of Channel Confluences. J. Geol. https://doi.org/10.1086/628230

Parsons, D.R., Best, J.L., Orfeo, O., Hardy, R.J., Kostaschuk, R., Lane, S.N., 2005. Morphology and flow fields of three-dimensional dunes, Rio Paraná, Argentina: Results from simultaneous multibeam echo sounding and acoustic Doppler current profiling. J. Geophys. Res. Earth Surf. 110, 1–9. https://doi.org/10.1029/2004JF000231

Petrie, J., Diplas, P., Nam, S., Gutierrez, M.S., 2010. Local boundary shear stress estimates from velocity profiles measured with an ADCP. River Flow 1749–1755.

Rennie, C.D., Villard, P.V., 2004. Site specificity of bed load measurement using an acoustic Doppler current profiler. J. Geophys. Res. 109, 1–15. https://doi.org/10.1029/2003jf000106

Rennie, C.D., Millar, R.G., 2004. Measurement of the spatial distribution of fluvial bedload transport velocity in both sand and gravel. Earth Surf. Process. Landforms 29, 1173–1193. https://doi.org/10.1002/esp.1074

Rennie, C. D., Church, M., 2010. Mapping spatial distributions and uncertainty of water and sediment flux in a large gravel bed river reach using an acoustic Doppler current profiler, J. Geophys. Res., 115, F03035. https://doi.org/10.1029/2009JF001556.

Rhoads, B.L., Kenworthy, S.T., 1995. Flow structure at an asymmetrical stream confluence. Geomorphology 11, 273–293. https://doi.org/10.1016/0169-555X(94)00069-4

Rhoads, B.L., Sukhodolov, N., 2001. Field investigation of three-dimensional flow structure. Water Resour. Res. 37, 2393–2410. https://doi.org/10.1029/2001WR000316

Rhoads, B.L., Sukhodolov, A.N., 2008. Lateral momentum flux and the spatial evolution of flow within a confluence mixing interface. Water Resour. Res. 44, 1–17. https://doi.org/10.1029/2007WR006634

Rhoads, B.L., Riley, J.D., Mayer, D.R., 2009. Response of bed morphology and bed material texture to hydrological conditions at an asymmetrical stream confluence. Geomorphology 109, 161–173. https://doi.org/10.1016/j.geomorph.2009.02.029

Rhoads, B.L., Johnson, K.K., 2018. Three-dimensional flow structure, morphodynamics, suspended sediment, and thermal mixing at an asymmetrical river confluence of a straight tributary and curving main channel. Geomorphology 323, 51–69. https://doi.org/10.1016/j.geomorph.2018.09.009

Riley, J.D., Rhoads, B.L., 2012. Flow structure and channel morphology at a natural confluent meander bend. Geomorphology 163–164, 84–98. https://doi.org/10.1016/j.geomorph.2011.06.011

Riley, J.D., Rhoads, B.L., Parsons, D.R., Johnson, K.K., 2015. Influence of junction angle on three-dimensional flow structure and bed morphology at confluent meander bends during different hydrological conditions. EARTH Surf. Process. LANDFORMS 40, 252–271. https://doi.org/10.1002/esp.3624

Sassi, M.G., Hoitink, A.J.F., Vermeulen, B., Hidayat, 2011. Discharge estimation from H-ADCP measurements in a tidal river subject to sidewall effects and a mobile bed. Water Resour. Res. 47, 1–14. https://doi.org/10.1029/2010WR009972

Shugar, D.H., Clague, J.J., 2011. The sedimentology and geomorphology of rock avalanche deposits on glaciers. Sedimentology 58, 1762–1783. https://doi.org/10.1111/j.1365-3091.2011.01238.x

Sime, L.C., Ferguson, R.I., Church, M., 2007. Estimating shear stress from moving boat acoustic Doppler velocity measurements in a large gravel bed river. Water Resour. Res. 43, 1–12. https://doi.org/10.1029/2006WR005069

Stutenbecker, L., Delunel, R. Schlunegger, F., Silva, T.A., Šegvić, B., Girardclos, S., Bakker, M., Costa, A., Lane, S.N., Loizeau, J.-L., Molnar, P., Akçara, N. and Christl, M., 2018. Reduced sediment supply in a fast eroding landscape? A multi-proxy sediment budget of the upper Rhône basin, Central Alps. Sedimentary Geology, 375, 105-19

Sukhodolov, A.N., Krick, J., Sukhodolova, T.A., Cheng, Z., Rhoads, B.L., Constantinescu, G.S., 2017. Turbulent flow structure at a discordant river confluence: Asymmetric jet dynamics with implications for channel morphology. J. Geophys. Res. Earth Surf. 122, 1278–1293. https://doi.org/10.1002/2016JF004126

Sukhodolov, A.N., Sukhodolova, T.A., 2019. Dynamics of Flow at Concordant Gravel Bed River Confluences: Effects of Junction Angle and Momentum Flux Ratio. J. Geophys. Res. Earth Surf. 124, 588–615. https://doi.org/10.1029/2018JF004648

Szupiany, R.N., Amsler, M.L., Best, J.L., Parsons, D.R., 2007. Comparison of fixed- and moving vessel measurements with an aDp in a large river. Journal of Hydraulic Engineering, 133, 1299–1309.

Tang, W., Hong, J., Huang, X., Huang, J., 2018. Key issues on seepage analysis in mountain river embankment. IOP Conf. Ser. Earth Environ. Sci. 189 052041. https://doi.org/10.1088/1755-1315/189/5/052041

Venditti, J., G., Rennie, C.D., Bomhof, J., Bradley, R.W., Little, M., Church, M., 2014. Flow in a bedrock canyon. Nature, 513:534-537, https://doi.org/10.1038/nature13779.

Vermeulen, B., Sassi, M.G., Hoitink, A.J.F., 2014b. Improved flow velocity estimates from moving-boat ADCP measurements. Water Resources Research, 50, 4186–4196.

Yuan, S., Tang, H., Li, K., Xu, L., Xiao, Y., Gualtieri, C.,Rennie, C., Melville. B. Hydrodynamics of a large confluence: Flow, suspended sediment transport

andmorphological features. Water Resources Research, https://doi.org/10.1029/2020WR028284,2021

https://www.bafu.admin.ch/bafu/fr/home/themes/eaux/etat/donnees/statistiques-des-crues.html